Spectroscopic manifestations of the Kondo effect on single adatoms

2009 J. Phys.: Condens. Matter 21 053001

(http://iopscience.iop.org/0953-8984/21/5/053001)

IOP Publishing Journal of Physics: Condensed Matter

J. Phys.: Condens. Matter **21** (2009) 053001 (19pp) doi:10.1088/0953-8984/21/5/053001

TOPICAL REVIEW

Spectroscopic manifestations of the Kondo effect on single adatoms

Markus Ternes[1,2], Andreas J Heinrich[1] and Wolf-Dieter Schneider[2]

[1] IBM Almaden Research Center, 650 Harry Road, San Jose, CA, USA
[2] Institut de Physique des Nanostructures, École Polytechnique Fédérale de Lausanne, CH-1015 Lausanne, Switzerland

E-mail: markus.ternes@epfl.ch

Received 10 October 2008, in final form 25 November 2008
Published 19 December 2008
Online at stacks.iop.org/JPhysCM/21/053001

Abstract

The present topical review focuses on recent advances concerning an intriguing phenomenon in condensed matter physics, the scattering of conduction electrons at the localized spin of a magnetic impurity: the Kondo effect. Spectroscopic signatures of this effect have been observed in the past by high-resolution photoemission which, however, has the drawback of averaging over a typical surface area of 1 mm^2. By combining the atomic-scale spatial resolution of the scanning tunneling microscope (STM) with an energy resolution of a few tens of μeV achievable nowadays in scanning tunneling spectroscopy (STS), and by exposing the magnetic adatom to external magnetic fields, our understanding of the interaction of a single magnetic impurity with the conduction electrons of the nonmagnetic host has been considerably deepened. New insight has emerged by taking advantage of quantum size effects in the metallic support and by decoupling the magnetic adatom from the supporting host metal, for instance by embedding it inside a molecule or by separating it by an ultrathin insulating film from the metal surface. In this way, Kondo resonances and Kondo temperatures can be tailored and manipulated by changing the local density of states of the environment. In the weak coupling limit between a Kondo impurity and a superconductor only a convolution of tip and sample DOS is observed while for strongly coupled systems midgap states appear, indicating superconducting pair breaking. Magnetic impurities with co-adsorbed hydrogen on metallic surfaces show pseudo-Kondo resonances owing to very low-energy vibrational excitations detected by inelastic tunneling spectroscopy. One of the most recent achievements in the field has been the clarification of the role of magnetic anisotropy in the Kondo effect for localized spin systems with a spin larger than $S = 1/2$.

(Some figures in this article are in colour only in the electronic version)

Contents

1. The Kondo effect

The electrical resistance of pure metals usually decreases with decreasing temperature. This is a consequence of electron scattering due to lattice vibrations, which are gradually frozen out when reducing the temperature. However, already in the 1930s it was discovered that, in some metals containing magnetic impurities, the electrical resistance increases again below a certain temperature [1, 2]. The origin of this effect remained obscure for a long time and was finally explained in 1964 by Kondo [3, 4].

Kondo showed that these experimental observations can be understood within a scattering model, which takes explicitly into account the interaction of the spins of the conduction electrons of the host metal with the localized spin of the magnetic impurities (see figure 1). This behavior is termed 'the Kondo effect'. It only arises if the impurities are magnetic, i.e. if the total spin of all electrons of the impurity atom is unequal to zero.

A very intuitive model to describe a single magnetic impurity embedded in a nonmagnetic metallic host was given by Anderson [6]. The so-called 'Anderson single-impurity model' simplifies the full electronic structure by assuming only a single orbital state which can be filled with no, one or two electrons. For the prototypical transition metal cobalt (Co) with its odd number of 3d electrons (electronic configuration: $[\mathrm{Ar}]3\mathrm{d}^7 4\mathrm{s}^2$), this localized state is a d state, while for the prototypical rare earth metal cerium (Ce) with its single 4f electron (electronic configuration: $[\mathrm{Xe}]4\mathrm{f}^1 5\mathrm{d}^1 6\mathrm{s}^2$) it is a 4f state. The singly occupied 4f state ($4\mathrm{f}^1$) is located below the Fermi energy at binding energy ϵ_f and is separated by the Coulomb repulsion energy U from the 4f state occupied with two electrons with opposite spins ($4\mathrm{f}^2$) as sketched in figure 2(a). Due to the hybridization between the 4f states and the continuum of electronic states in the metal host, the 4f levels are broadened by $\Delta = \rho_0 |V|^2$, with ρ_0 as the DOS at E_F of the supporting metal and V as the hybridization matrix element which couples the localized state with the continuum of band states.

Exchange processes can take place which flip the spin of the impurity from the 'up' to the 'down' state, or vice versa, as it is schematically shown in figure 1(a), while simultaneously a spin-excitation state close to the Fermi energy is created. In the framework of the Anderson model this process can be realized in two different ways: either first emptying the 4f state ($4\mathrm{f}^1 \rightarrow 4\mathrm{f}^0$) and then refilling it, or first putting a second electron into the 4f state ($4\mathrm{f}^1 \rightarrow 4\mathrm{f}^2$) and successively removing one electron. The final $4\mathrm{f}^1$ state, however, can be in the opposite spin state as compared to the initial one. These two processes are schematically drawn in figure 2(b).

While classically an energy of at least $-\epsilon_\mathrm{f}$ is necessary to bring the electron from the singly occupied $4\mathrm{f}^1$ state to an empty state in the metal at E_F, and an energy of at least $U + \epsilon$ is necessary to bring another electron from an occupied state in the metal at E_F into the $4\mathrm{f}^2$ state, in the quantum mechanical framework the Heisenberg uncertainty principle permits this excitation as a virtual process for a very short time of about $h/|\epsilon_\mathrm{f}|$ or $h/|\epsilon_\mathrm{f} + U|$, respectively [8]. Within this timescale of some femtoseconds (10^{-15} s), another electron has to tunnel from the occupied Fermi sea back to the impurity, or from the impurity back to the unoccupied part of the Fermi sea.

This spin exchange modifies the energy spectrum of the system. Taking many such processes together, a new ground state with lower total energy, the so-called Kondo resonance, is generated very close to the Fermi energy (see figure 3). This resonance is clearly a many-body phenomenon—the many electrons of the free-electron gas are decisive in the interaction with the localized state of the impurity: together they form the nonmagnetic Kondo singlet state in which the spin of the impurity is paired with the many electrons of the bulk continuum.

At $T = 0$ K the Kondo resonance near the Fermi energy has a half-width at half-maximum of Γ, which can be described by a characteristic temperature, the so-called Kondo temperature T_K:

$$T_\mathrm{K} = \frac{\Gamma}{k_\mathrm{B}} \approx \Gamma \times 11.6\ \mathrm{K\ meV^{-1}}, \tag{1}$$

and is expressed by the parameters of the system as [10]

$$\Gamma = k_\mathrm{B} T_\mathrm{K} \simeq \sqrt{2\Delta \frac{U}{\pi}} \exp\left[-\frac{\pi}{2\Delta} \left(\left| \frac{1}{\epsilon_\mathrm{f}} \right| + \left| \frac{1}{\epsilon_\mathrm{f} + U} \right| \right)^{-1} \right]. \tag{2}$$

The peak height has a strong temperature behavior and decays for $T \ll T_\mathrm{K}$ slowly with $1 - c(T/T_\mathrm{K})^2$ [11] but logarithmically for $T \gtrsim T_\mathrm{K}$ [12, 13]. Also the resonance width 2Γ depends on the temperature and is equal to equation (2) only at $T = 0$ and is, for finite temperatures, $2\Gamma = \sqrt{(\alpha k_\mathrm{B} T)^2 + (2 k_\mathrm{B} T_\mathrm{K})^2}$ [14, 15]. The linear growth of the width at $T \gg T_\mathrm{K}$ with α as the slope can be understood in the framework of the Fermi liquid model [11]. It is the result of the smearing of the Fermi–Dirac distributions for the initial and final sample electron states during the transition via the intermediate state for the processes depicted in figure 2(b), leading to a value of $\alpha = 5.4$ [16].

The Kondo effect and its theoretical foundations have now been known for quite a long time. The existence of the Kondo resonance in dense Kondo systems like solid surfaces or thin films of γ- and α-cerium as well as in Ce-heavy-fermion compounds has been experimentally confirmed by high-resolution photoemission electron spectroscopy (PES) [17–22] and by inverse photoemission [23, 24]. While these measurements always probe an ensemble of impurities due to the limited spatial resolution in PES, STM opened the unique opportunity to detect the Kondo effect in the smallest conceivable Kondo system: a single magnetic atom supported on top of a nonmagnetic metal. It was only in 1998 when the Kondo effect was detected on single adatoms using STM [25, 26] and in single quantum dots containing about 50 electrons by means of transport measurements [27, 13]. These fascinating results stimulated a genuine 'revival of the Kondo effect' [8]. (See also earlier reviews [28–30] on the subject.)

In general, STS measurements on magnetic atoms supported on metallic surfaces do not detect the Kondo peak in the spectral function close to E_F, but rather a dip-like structure as shown, for example, in figures 5 and 6 for measurements on single cobalt adatoms on Ag(100) and Cu(111).

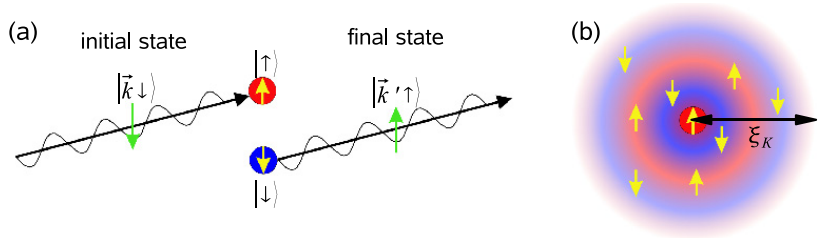

Figure 1. Kondo scattering on a single magnetic impurity [5]. (a) At sufficiently low temperatures an electron $|\vec{k}\downarrow\rangle$ of the host metal can be scattered at the impurity into the new state $|\vec{k}'\uparrow\rangle$ by spin exchange with the spin moment of the magnetic atom. While in (a) the dynamic of the spin-flip process is shown, the snapshot in (b) sketches the effect of this permanent flipping. The magnetic moment of the impurity is screened over the characteristic Kondo screening length ξ_K.

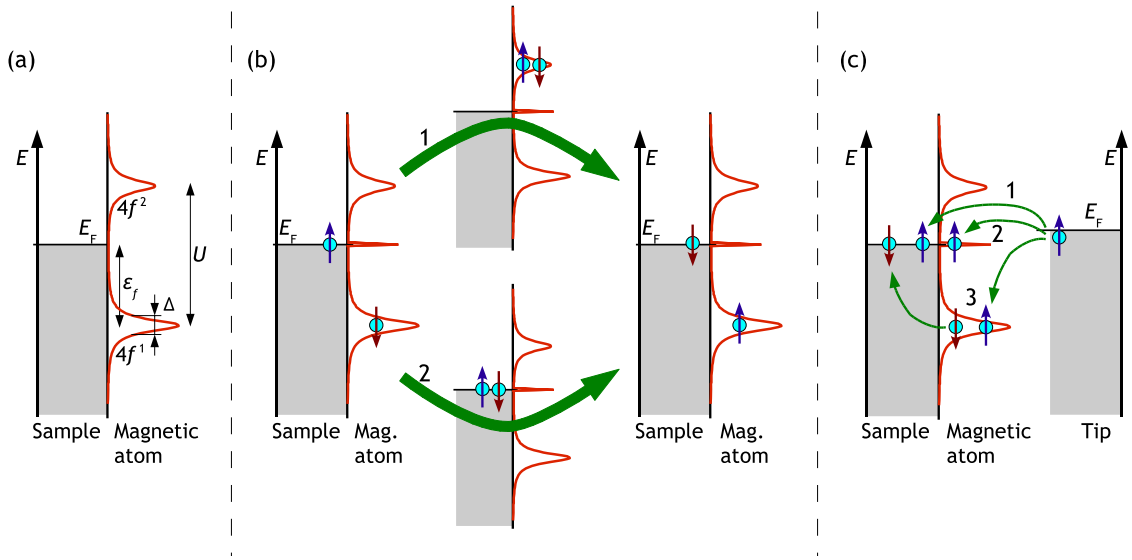

Figure 2. (a) Schematic drawing of the energy-dependent DOS in the experimental situation of a single magnetic adatom on a metal surface [7]. (b) The spin of the singly occupied 4f state can be flipped by a bulk electron of opposite spin via process 1 or 2 in which the adatom is either doubly occupied (process 1) or empty (process 2) during the intermediate step. These processes form the Kondo resonance close to E_F. (c) Electrons from a probing tip can now tunnel directly into empty states of the sample (1) or into the Kondo resonance (2). These tunnel processes conserve the electron spin while the third process is an indirect transition via a spin-flip process on the magnetic adatom (3).

To understand this behavior, we consider a situation as depicted in figure 2. A magnetic adatom (for example, Ce) is placed on top of a metal surface. The occupied $4f^1$ state is located below E_F, separated by U from the $4f^2$ state. At sufficiently low temperature the antiferromagnetic exchange interaction between electrons of the host metal and the localized magnetic state on the adatom creates a resonance close to E_F as described in figure 3. Electrons originating from the probing tip have now three possibilities to tunnel into the sample. They can tunnel directly into empty bulk states above E_F of the metal (path 1 of figure 2(c)), into the Kondo resonance which lies close to E_F (path 2) or indirectly via a spin-flip process into the hybridized and localized state of the magnetic adatom (path 3). The two different paths which conserve the spin (paths 1 and 2) are chosen by the tunneling electrons with probabilities given by the tunneling matrix elements t_1 and t_2 for tunneling into bulk states and the Kondo resonance, respectively. As a result, the tunneling current, being a coherent quantum effect, is determined by the quantum interference between both channels [7]. The third process (path 3), in which the electron from the tip tunnels directly to the orbitals of the adatom and changes its spin, will be of interest in section 6. Here we note that this process cannot contribute to the interference because it results in a final state with different spin. Thus, in typical STS experiments with weak tip–sample coupling, the tip acts as a true probe which does not influence the spectral function of the Kondo system. For tunnel junctions close to point contact this picture alters because now higher-order spin-flip processes are expected to additionally contribute to the interference [31].

Fano showed that the interference between both paths leads to an energy spectrum $\rho(E)$ which is described by the so-called Fano equation [32]:

$$\rho(E) \propto \rho_0 + \frac{(q+\epsilon)^2}{1+\epsilon^2}, \tag{3}$$

where ϵ is the normalized energy:

$$\epsilon = \frac{E - E_K}{\Gamma}, \tag{4}$$

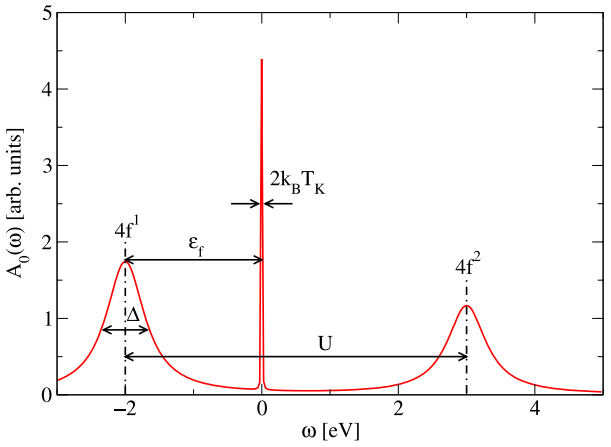

Figure 3. Simulation of the 4f spectral function $A_0(\omega)$ of a single magnetic impurity of cerium [5]. The singly occupied $4f^1$ state lies below the Fermi energy at ϵ_f and is broadened by Δ due to hybridization with the conduction electron gas of the host. The Coulomb repulsion U separates the unoccupied $4f^2$ state from the $4f^1$ state. The Kondo resonance occurs at approximately E_F and has a half-width at half-maximum of k_BT_K. Parameters used for the calculation after [9]: $\epsilon_F = -2$ eV, $U = 5$ eV and $\Delta = 0.34$ eV.

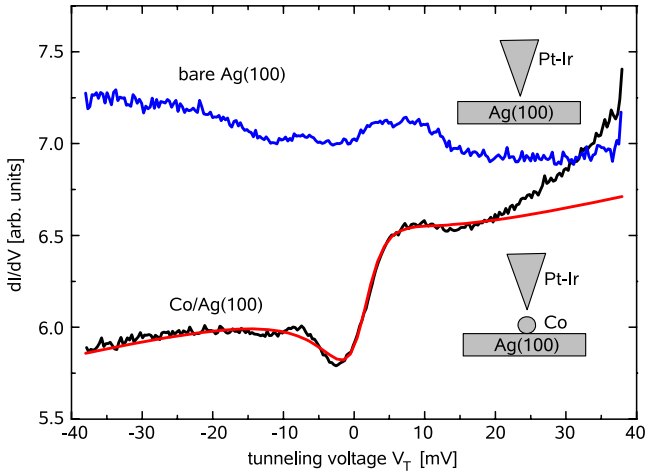

Figure 5. Kondo resonance measured on a single Co adatom on Ag(100) (lower curve) in comparison to the spectrum of the bare Ag(100) (upper curve) [5]. The data were obtained with a PtIr tip. The smooth curve (red) is a Fano fit to the lower curve with the best fit parameters of $q = 0.60 \pm 0.05$, $\Gamma = 8 \pm 1$ meV and $E_K = 3 \pm 2$ meV. Tunneling parameters before opening the feedback loop: $V_T = -46$ mV, $I_T = 0.5$ nA, $V_{mod} = 1$ mV, $T = 4.7$ K.

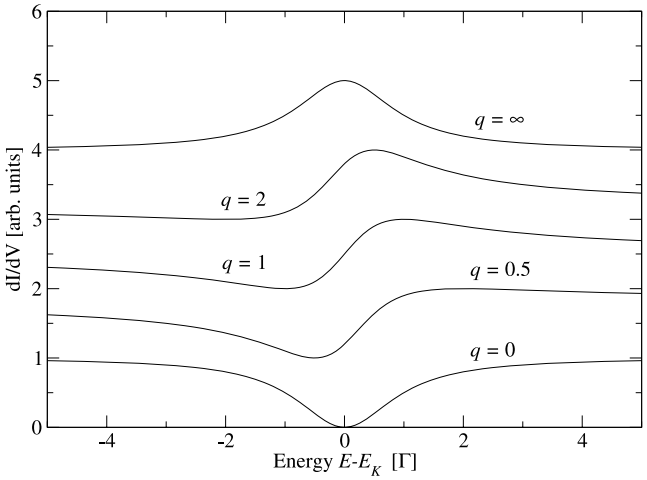

Figure 4. Set of curves calculated with the normalized Fano equation (5) for different q values. At $q = 0$ a Lorentzian dip is detected which corresponds to mainly direct tunneling. In the limit of large q a Lorentzian peak is formed corresponding to mainly indirect tunneling (see equation (6)). Intermediate values of q result in an S-like curve. All curves are shifted with respect to each other for clarity.

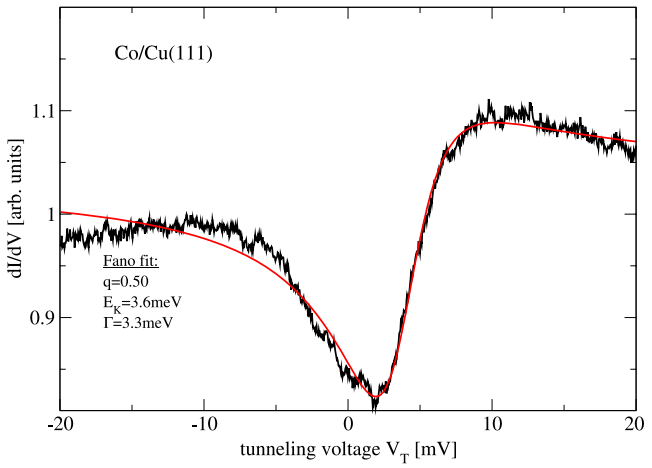

Figure 6. Kondo resonance measured on a single Co adatom on Cu(111) with an Ir tip and the corresponding Fano fit (smooth red curve) [5]. Tunneling parameters before opening the feedback loop: $V_T = -20$ mV, $I_T = 0.5$ nA, $V_{mod} = 0.28$ mV at a base temperature of $T = 1.2$ K. The parameters of the fit are given in the figure.

with E_K as the position and Γ as the half-width at half-maximum of the obtained curve. The lineshape of the curve described by equation (3) is determined by the form factor q which results for $q \to \infty$ in a Lorentzian peak and for $q = 0$ in a Lorentzian dip. The resulting lineshapes for a few intermediate q values are shown in figure 4.

Following a suggestion by Lutz, the appearance of a Fano lineshape in tunneling spectra of Kondo systems is easily understood by drawing a classical analogy in which the many-electron Kondo resonance around E_F is described by a weakly damped harmonic oscillator. The transfer function of this oscillator t_2, which is the ratio of response to a drive amplitude, is $t_2 = 1/(1 + i\epsilon)$. Here ϵ is defined as in equation (4) and $|t_2|^2 = 1/(1 + \epsilon^2)$ is the Lorentzian of the resonance. Now we add a constant to describe the direct tunneling of path 1. We will use without any restrictions $t_1 = -1/(1 - iq)$. STS detects the absolute square of the sum of t_1 and t_2, which is indeed the Fano equation (3):

$$|t_1 + t_2|^2 = \left| -\frac{1}{1 - iq} + \frac{1}{1 + i\epsilon} \right|^2 = \frac{1}{1 + q^2} \frac{(q + \epsilon)^2}{1 + \epsilon^2}. \quad (5)$$

The form factor q is given by the ratio between the direct and the indirect tunneling process at the resonance energy

E_K [7]:

$$q = \frac{t_2}{\pi \rho_0 V t_1} + \Lambda(\epsilon), \tag{6}$$

with V as the hybridization matrix element between the localized state and the continuum of the surface and $\Lambda(\epsilon)$ as a slowly varying parameter in energy and spatial location which accounts for the admixing of states from the continuum of the surface [32].

As the 4f orbitals of cerium are localized close to the nucleus of the adatom [33] owing to their centrifugal barrier, the tunneling probability t_2 into the Kondo resonance is strongly reduced compared to the probability t_1 to tunnel directly into the more extended s and p orbitals of the host metal [34]. Therefore, for measurements on Ce, q values close to zero are expected. To a first approximation, this argument holds also for the 3d states of magnetic transition metal adatoms. For example, from $\mathrm{d}I/\mathrm{d}V$ measurements on single Co adatoms supported on an Ag(100) or on a Cu(111) surface, as presented in figures 5 and 6, form factors of $q = 0.6$ and 0.5, are obtained, respectively.

In general, the quantitative analysis of a Kondo system in STS measurements is difficult. For example, the parameters of the Fano fit for the Co/Ag(100) and Co/Ag(111) systems (figures 5 and 6) were found to be different from values available in the literature [35–37]. The main problem as opposed to PES so far is the difficulty to detect the localized ionized 4f or 3d states and/or their crystal-field-split states directly with STS. Thus one is restricted to the analysis of the Kondo resonance close to E_F and a test of the resulting Anderson model parameters with higher-lying levels is not possible.

Unfortunately, the resonance signal in STS rarely has a well-formed Fano lineshape. Consequently, the fit of equation (3) to the obtained data results in different parameter sets depending on the assumed background and on the energy window of the data taken into account for the fit.

Another example for the difficulties to extract quantitative results from the lineshape analysis is the ongoing discussion of the influence of the surface state electrons on the Kondo resonance. While some authors conclude from their experiments that there is no or only a minor influence [35, 38], others infer from their analysis a clear indication for the Kondo scattering of surface state electrons [39]. Support for the latter finding is given by the detection of a quantum mirage Kondo resonance in the second focus of an elliptical corral on Cu(111), where only the first focus is occupied by a Co adatom [40].

In the quantitative analysis of the Kondo resonance, one important parameter is the average occupation number n_f for the 4f (3d) states of the adatom on the surface [10, 9]. While the atom has an integer number of 3d or 4f electrons in the gas phase, which is given by the nuclear charge and the position in the periodic table, the atom on top of a surface can exchange charge, leading to a higher or lower average occupation number in the 3d or 4f shell. The position of the Kondo resonance E_K (with its width Γ) is related to the occupation number n_f by [10]

$$E_K = \Gamma \tan\left(\frac{\pi}{2}(1 - n_f)\right). \tag{7}$$

The average occupation number n_f has the meaning of an extra charge which is transported from the host metal to the impurity or vice versa and ranges between $n_f = 0$ for the empty and $n_f = 2$ for the doubly occupied orbital in the Anderson impurity model. Furthermore, assuming a relatively small hybridization energy compared to the level energies, i.e.

$$\Delta \ll |\epsilon_f|, \qquad \Delta \ll |\epsilon_f + U|, \tag{8}$$

the average occupation number is calculated by the position of the $4f^1$ state and the Coulomb repulsion U [9]:

$$n_f = -\frac{\epsilon_f}{U} + \frac{1}{2}. \tag{9}$$

The charge transfer and hybridization Δ of the localized 4f (3d) states with the continuum of its host determine the Kondo temperature (according to equations (9) and (2)) and can be monitored by STS. The Kondo temperature changes with the number of available nearest neighbors on the supporting surface. An adatom has three nearest neighbors available for hybridization on (111) surfaces (assuming the adatom occupies a hollow site), while the nearest-neighbor number is increased to four on top of the (100) surface. This increase in hybridization leads to an increase of the Kondo temperature by ≈40% for Co atoms on Cu surfaces [35, 37]. Furthermore, embedded Co impurities in Cu(111) have been studied by growing epitaxial layers of Cu with ≈0.1% Co impurities on Cu(111) samples [41, 42]. Co atoms embedded in the first surface layer have 9 nearest neighbors and show a Kondo temperature of $T_K = 405 \pm 35$ K [41, 42] which is close to the bulk value of ≈530 K [43] in which the Co impurity is surrounded by 12 nearest neighbors. Also the number of ligands, such as, for example, CO, bound to the magnetic adatom influences the coupling of the local magnetic moment with the metallic surface and thus the Kondo temperature [44].

Here we note that recent spectroscopic results on small $CoCu_n$ clusters, fabricated by atom manipulation on Cu(111), show that the simple scaling of the Kondo temperature with the number of next neighbors or ligands is not sufficient to describe all observations [45]. The Kondo temperature in these experiments increased almost linearly for $CoCu_n$ clusters with $n = 0$–2 but was found to decrease again for $n = 3$–4 Cu atoms per cluster. These results were accounted for by a change in the LDOS at E_F which changes the amount of hybridization and thus the Kondo temperature. This outcome demonstrates the importance of the local electronic structure for correlation effects in small clusters.

In this context, metal–organic complexes, like Co–phthalocyanine, are interesting objects to study. For example, they permit us to change the Kondo temperature of the magnetic atom in the center of the complex by a controlled removing of external hydrogen atoms [46]. In this case the coupling between the magnetic adatom and the metallic host is still strong enough to allow for Kondo scattering, but the molecular orbitals inhibit sufficiently the direct tunneling path to the metal surface. As a consequence, increased q values result in the Fano equation (3), which lead to the observation of a Kondo peak and not a Kondo dip in the STS spectra.

In a closely related experiment, magnetic Fe–phthalocyanine molecules have been deposited on Au(111). Depending on the position of the magnetic adatom with respect to the substrate (atop of a Au surface atom or in a bridge position), a Kondo peak or a Kondo dip were observed. This behavior was attributed to the change in the Kondo temperature owing to the adsorption-site-dependent change in the local density of states [47]. In a related work, the Kondo resonance of individual Mn–phthalocyanine molecules adsorbed on Pb islands grown on Si(111) was studied by STS. Oscillating Kondo temperatures as a function of the lead film thickness were observed and were attributed to the formation of quantum-well states in the host islands [48]. Subsequently, the influence of quantum-well states via the variation of the density of states at the Fermi level on the oscillation of the Kondo temperature has also been observed for Co adatoms on Cu/Co/Cu(100) multilayers [49].

Furthermore, in going from tunneling to point contact with an STM tip on a Co adatom supported on a Ag surface, a concomitant increase of the Kondo temperature was observed, indicating the clear influence of the changed local density of states which shifts the 3d levels of the Co atom closer to the Fermi energy and increases their broadening, i.e. their hybridization with the bulk continuum [31].

As long as the assumptions in equation (8) are fulfilled, the above outlined model is sufficient to describe the Kondo effect for a wide range of different adatom–substrate systems. This is in contrast to the still ongoing theoretical discussion [50–52] to explain the STS spectra on strongly hybridized adatoms such as, for example, Ti and Ni [14, 53]. In these and in similar systems the full impurity Green's function $G_{\mathrm{d,f}}(\omega)$ [10]:

$$G_{\mathrm{d,f}}(\omega) = \frac{\Gamma/\Delta}{\omega - E_{\mathrm{K}} + \mathrm{i}\Gamma}, \qquad |\omega| \lesssim T_{\mathrm{K}}, \quad T = 0, \quad (10)$$

has to be used together with the term $V^2 G_{\mathrm{d,f}}(\omega) \equiv T_c(\omega)$ which is the T matrix of the conduction electrons, as it follows from the Anderson Hamiltonian [9]. The complex lineshape observed in tunneling experiments on Ti/Au(111) and Ti/Ag(100) [14, 53] is then due to the multiple Kondo resonances arising from the crystal-field-split local orbitals of the transition metal impurity [52, 54] and can be calculated using equation (10) in the Dyson equation:

$$G_{\mathrm{d,f}}(\omega) = G^0_{\mathrm{d,f}}(\omega) + G^0_{\mathrm{d,f}}(\omega) T_c(\omega) G^0_{\mathrm{d,f}}(\omega). \quad (11)$$

Finally, one has to remark that the dynamical spin-flip between the localized magnetic adatom and the electrons of the Fermi sea leads to spin-polarized electron waves (spin waves) in the supporting metal (see figure 1(b)) [55–57].

The characteristic length scale, the so-called Kondo screening length ξ_{K}, in which the impurity spin is antiferromagnetically screened, is given by [10]

$$\xi_{\mathrm{K}} = \frac{\hbar v_{\mathrm{F}}}{k_{\mathrm{B}} T_{\mathrm{K}}}, \quad (12)$$

with $v_{\mathrm{F}} = \sqrt{\frac{2E_{\mathrm{F}}}{m^*}}$ the Fermi velocity of the electrons in the host. In a simplified picture ξ_{K} represents the extension of the many-particle singlet state formed between the localized magnetic moment and the spin of the host electrons. For typical metals such as Ag and Cu with $v_{\mathrm{F}} \approx 10^6$ m s^{-1} [58], and Kondo temperatures which range from 10–100 K for adsorbates such as, for example, Co, ξ_{K} becomes relatively large with 100–10 nm. Thus, it is indeed possible that interactions between well-ordered single adatoms, such as, for example, in superlattices [59–61], may lead to the creation of a Kondo lattice in which the spin-flip between individual adatoms is correlated. Nevertheless, direct experimental evidence of the Kondo screening cloud has not yet been detected. One reason might be that the polarization of the screening electrons is very small owing to the large volume of the Kondo sphere. With $\xi_{\mathrm{K}} = 100$ nm, the Kondo sphere would contain more than 2×10^8 atoms [57].

2. The Kondo resonance on Ce adatoms revisited

The electronic and magnetic properties of Ce show extreme variations with temperature and pressure, which is unique among elemental solids [24]. At ambient conditions, solid Ce is in the γ-phase with a magnetic susceptibility of $\chi \approx 4.8 \times 10^{-3}$ and a Kondo temperature of $k_{\mathrm{B}} T_{\mathrm{K}} \approx 10$ meV [62, 63]. At high pressure or low temperature the γ-phase collapses into the α-phase with an isostructural volume reduction of up to 17% [64] and a concurrent decrease of its magnetic susceptibility to $\chi \lessapprox 0.4 \times 10^{-3}$ and an increase in Kondo temperature to $k_{\mathrm{B}} T_{\mathrm{K}} \approx$ 200–250 meV [65]. Measurements using high-resolution photoemission electron spectroscopy (PES) on ultrathin Ce layers show reduced Kondo temperatures of $k_{\mathrm{B}} T_{\mathrm{K}} \approx 5$ meV and $k_{\mathrm{B}} T_{\mathrm{K}} \approx 26$ meV for γ-Ce and α-Ce, respectively [17, 19].

These intriguing bulk properties and the PES results stimulated the early investigations of the Kondo effect on Ce adatoms on an Ag(111) surface [25], where a characteristic dip in the tunneling spectra was found around the Fermi energy (see figure 7). This dip has been attributed to the manifestation of the Kondo effect via a Fano antiresonance with a Fano form factor $q = 0$. The width of the Kondo dip was found to be $k_{\mathrm{B}} T_{\mathrm{K}} \approx$ 20–30 meV, which is considerably lower than the value for bulk α-Ce. This result was, in principle, consistent with the expected decrease in hybridization with decreasing Ce coordination. On the other hand, an even more pronounced decrease in $k_{\mathrm{B}} T_{\mathrm{K}}$ for a single Ce adatom on top of an Ag surface could have been anticipated. Furthermore, the recent achievement of the creation of a hexagonal superlattice of Ce adatoms on an Ag(111) surface [59–61] cast doubts on the claim to have observed the Kondo resonance on a single Ce adatom. During these experiments, single Ce adatoms were found to diffuse on the Ag(111) surface even at temperatures as low as 4 K, leading to the formation of dimers and larger clusters (see reference 19 in [59]). This unsatisfactory situation motivated us to investigate the spectroscopic response of a single Ce adatom with high-resolution STS using an STM under UHV conditions in a ^{3}He Joule–Thomson refrigerator with a base temperature of 0.56 K [66].

To this end, single Ce adatoms have been deposited on a bare Cu(100) surface and on an ultrathin insulator, CuN on Cu(100). The results of these new measurements are: a single

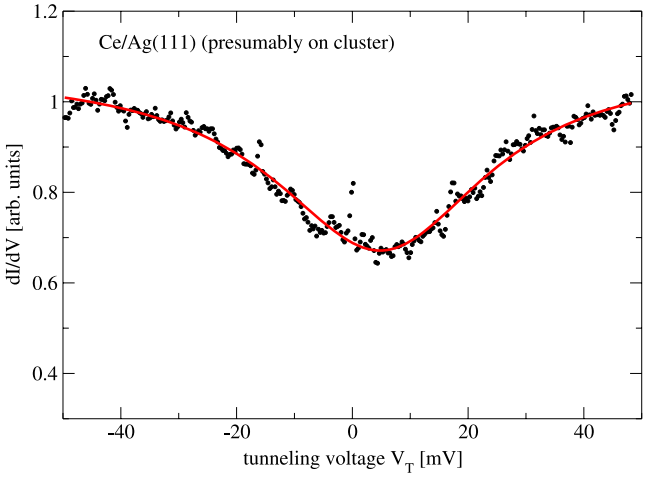

Figure 7. Spectra measured presumably on a Ce cluster adsorbed on Ag(111) at a temperature of 4.7 K (see text). The full line (red) is a Fano fit with a half-width at half-maximum of $\Gamma = 23$ mV. Data taken from [25].

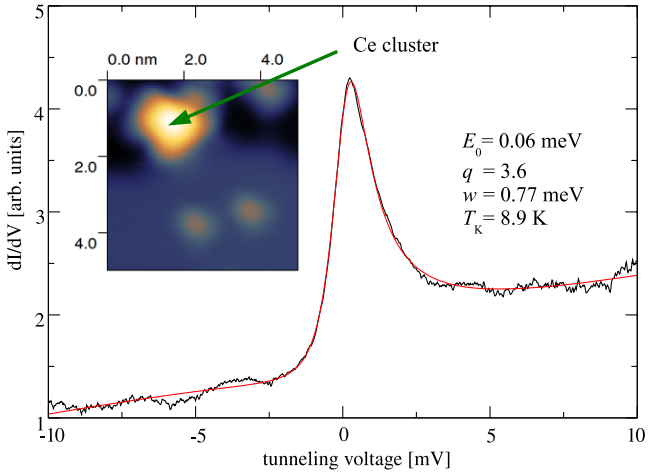

Figure 8. Kondo resonance measured on a Ce cluster of >2 Ce atoms on CuN (see the inset) with an Ir tip and the corresponding Fano fit (smooth red curve). Tunneling parameters before opening the feedback loop: $V_T = -20$ mV, $I_T = 0.5$ nA, $V_{mod} = 0.28$ mV at a base temperature of $T = 0.5$ K. The parameters of the fit are given in the figure.

Ce adatom shows no Kondo resonance, neither on Cu(100) nor on CuN. Consequently $k_B T_K$ must be sufficiently smaller than 0.3 meV for a single Ce adatom. However, Ce clusters of more than 2 atoms per cluster show a very narrow Kondo resonance with a Kondo temperature of $k_B T_K \approx 1$ meV, as illustrated in figure 8. In the light of these new results we have to conclude that the observation of the Kondo resonance for Ce on Ag(111) [25] has been made on Ce clusters and not on single Ce adatoms.

The strong reduction of the Kondo temperature for thin layers and for single atoms as compared to Kondo temperatures in the corresponding solids is observed in all Kondo systems. For instance, single Co adatoms supported on noble metal surfaces reveal a Kondo temperature of $T_K = 30$–100 K in STS [26, 35, 37] (see also figures 5 and 6), which is much lower than the bulk Kondo temperature of $T_K \approx 1000$ K [67–69]. The reduction of the number of available neighbors in dimensionally reduced systems leads to a decrease of hybridization of the magnetic impurity with the bulk electronic system of the supporting crystal [70].

3. Pseudo-Kondo resonances: observation of very low-energy vibrations

Typically, STM and STS experiments on single adatoms or single molecules are performed in ultra-high vacuum (UHV) at temperatures below $T = 10$ K, where the presence of hydrogen in the tunneling region may lead to surprising spectroscopic signatures, depending on the adsorbate concentration and on the tunneling parameters. Gupta *et al* [71] observed on a Cu(111) surface differential conductance (dI/dV) spectra ranging from those reminiscent of an energy gap in a superconductor to ones with negative differential resistance features, characteristic for vibrational excitations of an adsorbed molecule on a surface [72]. These findings were a motivation for a detailed study of the role of the low-temperature co-adsorption of hydrogen on single adatoms of Ce, lanthanum (La) and chromium (Cr) on Ag(100) [73].

The experiments were performed in a low-temperature STM in UHV at a temperature of $T = 4.9$ K [74]. Ce, La and Cr atoms were thermally evaporated from pure metal ingots wound in a tungsten filament and deposited onto a well-prepared Ag(100) surface.

In figure 9(a), obtained on Ag(100) with a Ce adatom concentration of 5×10^{-4} monolayer (ML) at a bias voltage of $V_T = -100$ mV, two different adsorbate species are clearly distinguishable. While about 50% of the objects on the surface are stable, the remaining ones display a 'fuzziness' during the horizontal tip scan. Figure 9(b) illustrates the bias-voltage-dependent imaging. During scanning at tunneling voltages V_T between -90 and $+120$ mV the unstable adsorbates 'B' are imaged as large protrusions of typically 210 ± 10 pm apparent height, only slightly smaller than the stable ones 'A' of about 230 ± 10 pm height, determined from an analysis of 700 adsorbates. By contrast, scanning at bias voltages below $V_T = -90$ mV or at $+120$ mV $< V_T < +200$ mV reveals several reversible transitions of the object from a large apparent height of 210 ± 10 pm to a small one of 95 ± 10 pm and vice versa. The switching object spontaneously returns back to its large state once the tip is removed during scanning, as is clearly visible in figure 9(b). Scanning at bias voltages above $+200$ mV images the object in its large state. The instability in the line scan indicates small lateral displacements of the adsorbate under the tip. The switching to the small state is found for both bias polarities, indicating that the electrostatic interaction between tip and adsorbate creates an induced dipole [75]. However, the effect is not symmetric, as at positive bias voltages larger than $+200$ mV the adsorbate returns to its large state. Therefore also quadrupolar electrostatic interactions at least have to be present. Data from different Ag(100) samples with varying Ce coverages ($\leqslant 0.001$ ML) and different tips (PtIr, W) show that between 1 and 50% of all adsorbates are switchable, while the

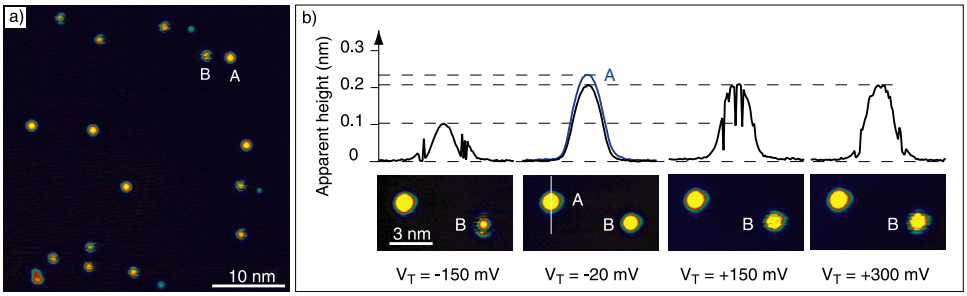

Figure 9. (a) STM image of a 5×10^{-4} monolayer (ML) Ce on Ag(100) at a temperature of 4.9 K revealing two different adsorbate species at the surface: a stable one A and an unstable switching object B. Scanning is horizontally line-by-line from bottom to top ((a) and (b)). Image size: 40×40 nm^2, $V_T = -100$ mV, $I_T = 50$ pA. (b) Cross sections (as indicated by the vertical white line in the topography at $V_T = -20$ mV) and STM topographies of the two objects A and B at different bias voltages, showing the switching behavior in the apparent height of object B. From [73].

remaining ones are stable. Cr and La adsorbates show similar switching characteristics, Cr adsorbates typically switch at bias voltages of +300 mV.

In order to identify the chemical nature of the adsorbates, many evaporation cycles with the hot tungsten filament were performed. The number of switchable objects decreases to less than 1% after numerous outgassing and deposition cycles accompanied by a concomitant decrease of the hydrogen partial pressure as detected by mass spectroscopy. This finding indicated the presence of hydrogen on the sample. In addition, STM revealed a number of depressions on the bare Ag(100) surface, characteristic of atomic hydrogen adsorption [76–78]. Additional experimental evidence for the presence of hydrogen on the sample was obtained from the following observation: applying short positive voltage pulses (+4 V, 50 ms) to the adsorbates, the unstable adsorbates are transformed into stable objects, pointing towards a tip-induced detachment of hydrogen [79, 46]. Moreover, a switching object can be laterally displaced by several nm, indicating molecular bonding between Ce and H. Consequently, the origin of the observed surprising switching phenomenon of the adsorbates was attributed to the presence of hydrogen. Atomic hydrogen coadsorbs (in the gas phase, by dissociative adsorption at the metal adatom sites, or by tip-induced diffusion in the presence of the electric field between tip and sample [75, 80]) at the Ce, La or Cr atoms. This hydrogen co-adsorption distinguishes the switchable objects from the stable ones. The former are identified as metal-monohydride molecules (MeH) and the latter as bare metal adatoms. The intriguing switching behavior at a threshold bias voltage indicates a flipping between two characteristic conformations of the molecule on the surface induced by the electric field in the STM junction [72, 75, 81, 82].

Once switched to the small state, the MeH molecule remains in this state even at reduced absolute tunneling voltage below the switching voltage of ≈100 mV as long as the tip is maintained above the molecule. Evidently, in addition to the electric field, a van der Waals force is acting between tip and molecule. This characteristic behavior allows us to obtain spectroscopic data of the molecule in its two states.

If the tip is placed above the CeH molecule in its large state, the measured differential conductance $\mathrm{d}I/\mathrm{d}V$ is rather featureless and constant around the Fermi energy E_F, as indicated in figure 10(a)(1). In contrast, if the $\mathrm{d}I/\mathrm{d}V$ spectrum is taken on the same molecule after being switched to the small state, a pronounced depletion of about 20% around E_F, with a full width at half-maximum (FWHM) of ≈6 meV, is observed (figure 10(a)(2)). Similar symmetric dips around E_F are observed for LaH and CrH molecules in their small state (figure 10(a)). As this dip is also present for LaH, which bears no occupied 4f states, an interpretation of this feature in terms of a Kondo resonance has to be discarded. Consequently, the observed spectral features are identified as vibrational excitations. Measurements with varying tunneling resistances give essentially identical results, indicating an inelastic tunneling process in the non-saturated regime [71].

The $\mathrm{d}I/\mathrm{d}V$ spectrum for such an IET process can be expressed as [16, 83, 71, 5]

$$\left.\frac{\mathrm{d}I_T}{\mathrm{d}V}\right|_{V_T} = \sigma_e + \sigma_i \left[F\left(\frac{-eV_T + E_i}{k_B T}\right) + F\left(\frac{eV_T + E_i}{k_B T}\right)\right] \tag{13}$$

where σ_e and σ_i denote the elastic and inelastic linear conductance, respectively, E_i is the excitation energy and F is a function defined by $F(x) = [1 + (x-1)\exp(x)]/[\exp(x) - 1]^2$. The spectral lineshape shows a step-like increase of width $5.4k_BT$ in the conductivity at excitation energies $\pm E_i$ with respect to E_F. A simulation of the data with equation (13) yields good agreement between experiment and model, as shown in figure 10 (red). Consequently, we identify the spectral feature as a vibrational mode of ≈3 meV and ≈7 meV excitation energy for the CeH (LaH) and CrH molecules, respectively.

A careful inspection of high-resolution images reveals that the molecule in its small state is always at the same position on the surface when switched from large to small. However, as shown in figure 10(b), after a switching event, the center of the molecule in its large state is found displaced by about 0.1 nm (Ag lattice constant: 0.289 nm) as compared to its former position in its large state.

Four different positions of the molecule in its large state are observed on the Ag(100) surface which hints at the geometrical arrangement of the CeH molecule on Ag(100), as proposed in figure 10(c). Here, the hydrogen atom is supposed

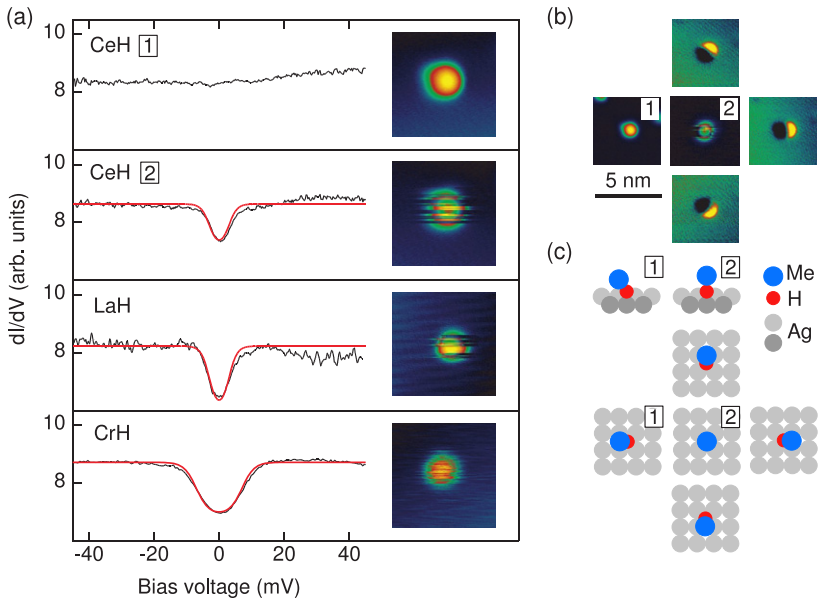

Figure 10. (a) $\mathrm{d}I/\mathrm{d}V$ spectra and STM topographies of metal monohydrides. CeH in its state with large (1) and small (2) apparent height, as well as LaH and CrH in their small apparent height recorded at $T = 4.9$ K. Tunneling spectroscopy parameters: $V_{\mathrm{mod}} = 1$ mV, $I_{\mathrm{T}} = 500$ pA. Simulation of the data (smooth red line) using equation (13) yields an excitation energy $E_{\mathrm{i}} \approx 3$ meV for Ce and La and ≈7 meV for Cr. (b) One switching molecule, observed in its small state (2) at $V_{\mathrm{T}} = -100$ mV and in its large state (1) at $V_{\mathrm{T}} = -20$ mV. The three other equivalent large configurations are revealed by displaying the height differences with respect to configuration (1). (c) Ball model (top and side views) showing the geometry of the MeH molecule adsorbed on Ag(100) in its small (2) and large (1) apparent state.

to occupy a fourfold hollow site and the CeH molecule is lying on the surface. The small state is assumed to correspond to a conformation where the molecular axis is perpendicular to the surface, a configuration stabilized by the tip. However, once the tip is removed, the molecule returns to its large state, for which four equivalent orientations on the surface are observed, as sketched in figure 10(c). A scenario, where the relative positions of hydrogen and Ce are interchanged, might also be possible. However, as vibrational excitations for H adsorbed on a metal surface are typically larger than 50 mV [78], which we do not observe, this configuration seems to be less probable.

Spin-flip excitations, as observed recently for single Mn atoms on an ultrathin oxide layer [66, 84], have to be excluded in the present case where the adsorbates are in direct contact with a metallic surface. It is interesting to note that the vibrational excitation energy for CeH and CrH molecules scales roughly with the inverse square root of the atomic masses, confirming the vibrational origin of the observed spectral feature. The fact that the vibrational excitation is only observed when the metal-monohydride molecules are in the small state can be attributed to two factors: (i) the local electronic structure for the two molecular conformations is different in order to selectively allow for the excitation of vibrational mode of specific symmetry and (ii) the large conductance drop when passing from large to small apparent height of the molecule is accompanied by a corresponding large increase of the ratio between inelastic and elastic contributions to the current, making these excitations measurable [85]. Recently, a theoretical investigation of this switching phenomenon as well as of the very-low-lying vibrational excitations has been performed [86].

Typical internal vibrational modes for free CrH and LaH molecules are in the range of 200 meV [87, 88]. Furthermore, for example, for single Co adatoms on a Cu single crystal surface the vertical stretch mode is predicted to have an energy of 33 meV [89]. Consequently, these modes cannot be responsible for the low-energy vibrations detected in the present experiment. However, very-low-energy vibrational modes have been observed, for example, for CO molecules and for Co adatoms on Cu surfaces in an energy range between 3 and 6 meV. They have been assigned to external frustrated translational modes, where the molecule or atom vibrates parallel to the surface [90, 81, 89]. Therefore, we tentatively identify the observed inelastic vibrational excitation for the MeH molecules with a frustrated translational mode on the Ag(100) surface.

We note that hydrogen co-adsorption has also been observed for single Co adatoms [5]. The Co atoms were deposited on a Cu(111) sample. Subsequently, atomic and molecular hydrogen was dosed from a heated tungsten filament. By placing the filament directly over a mass spectrometer it was verified that only hydrogen, which originates from hydrogen incorporations in the tungsten wire, was evaporated. A constant-current topographic image of the Cu(111) surface after dosing hydrogen with the filament is shown in figure 11(a). On top of the 20 × 20 nm^2 large detail of the Cu(111) surface, seven adsorbates are visible as protrusions. The native Co adatoms have an apparent height of about 90 pm, as indicated by the apparent height of the protrusion located at 1.5 nm in figure 11(b) and show a Fano resonance close to the Fermi energy in the spectrum (see figure 6) due to Kondo screening. The two protrusions marked by circles in the image have a lower apparent height of only

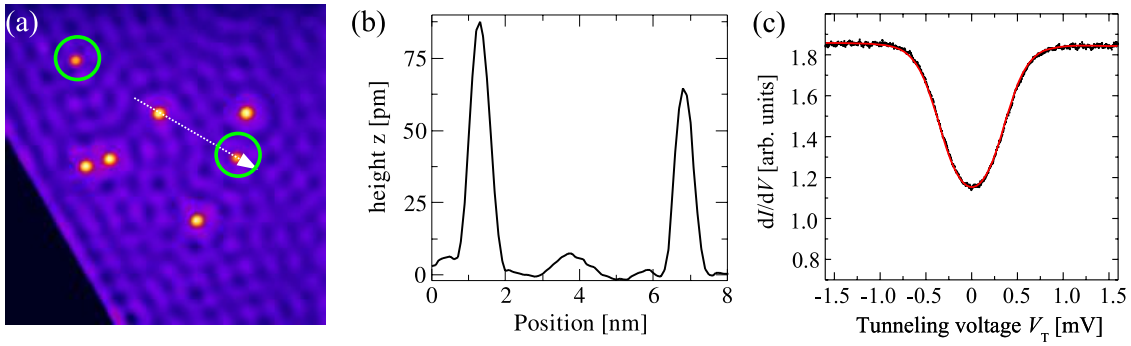

Figure 11. (a) STM Image of individual Co adatoms (bright protrusions) on top of a Cu(111) surface after dosing of hydrogen on the cold sample. Image parameters: 20×20 nm^2, $V_T = -20$ mV, $I_T = 1$ nA, $T = 0.6$ K. The periodic height modulations of a few pm amplitude are due to interferences between surface state electrons, which are reflected at a Cu(111) step edge (bottom left) and at the adsorbates, leading to standing wave patterns. (b) A height profile along the arrow in (a) reveals two different species with different apparent heights. The smaller ones are marked with circles in (a). (c) STS (setpoint: $V_T = -2$ mV, $I = 1$ nA, $V_{mod} = 28$ μV) measured on the species with smaller apparent height (dots: data, smooth red line: fit to equation (13)). The larger species show a different spectrum similar to figure 6. From [5].

≈65 pm, as illustrated for the protrusion located at 7 nm in figure 11(b). The latter were identified as Co-monohydride molecules which show no Kondo resonance but a symmetric dip around E_F with a half-width of only 325 ± 25 μV, characteristic for a vibrational excitation (figure 11(c)).

We note that the presence of hydrogen in the tunnel junction of an STM also has other astonishing consequences for the detection of physical properties of the system under investigation. For example, hydrogen adsorption on the apex of a Cr tip leads to a giant spin contrast for double-layer Co islands on Pt(111) [91]. Adding molecular hydrogen below its condensation temperature to the tunneling junction of a low-temperature STM resulted in a novel imaging method achieving ultra-high geometrical resolution on certain adsorbed molecular species. The STM contrast could be switched between the conventional mapping of the electronic local density of states and the new geometric imaging by selecting the appropriate bias voltage [92].

4. Probing the Kondo effect of individual magnetic adatoms with a superconducting tunneling tip

The pioneering discovery of the presence of spin-polarized quasiparticle excitations in the energy gap of a superconductor [93], induced by magnetic impurities (Mn, Gd) supported on an Nb single crystal and measured with a normal metal Au tunneling tip [94] opened a new avenue for the investigation of the interactions between magnetism and superconductivity on a local scale. Subsequently, a mirror experiment has been performed where the role of tip and sample have been interchanged: a superconducting Nb cluster attached to an Au tip was used to monitor the local influence of a magnetic cluster (Gd trimer) supported on a normal metal surface (Cu(100)) on the superconducting properties of the tip [95]. However, as these measurements have been performed at temperatures of about 3.8 K, the Bardeen–Cooper–Schrieffer (BCS) gap [96] of the Nb tip is not yet very pronounced, which makes the detection of possible quasiparticle excitations within the gap more difficult. Only after subtraction, division or deconvolution of the tunneling spectra obtained on the impurity and on the bare metallic surface have these excitations been extracted. This situation can be improved considerably using an STM which operates at a temperature of 0.6 K. Now the BCS gap of the Nb-tunnel tip is essentially developed [97], facilitating the direct observation of quasiparticle excitations induced by magnetic impurities in the gap. Thus a low-temperature STM equipped with a superconducting tunneling tip may become an ideal tool not only for the local detection of supported magnetic impurities but also as a source or drain for spin-polarized electrons.

The measurements were performed using an STM under UHV conditions in a ^{3}He Joule–Thomson refrigerator with a base temperature of 0.56 K [66]. Co was deposited on a well-prepared Cu(111) single-crystal surface. By indenting an Ir tip between 1 and 20 μm into an Nb(110) single crystal, cleaned by successive cycles of heating and Ar-ion sputtering, an Nb microcrystal was attached on the apex of the tip. Using these tips, spectroscopic $\mathrm{d}I/\mathrm{d}V$ measurements were performed with a standard lock-in technique.

The $\mathrm{d}I/\mathrm{d}V$ spectrum depicted in figure 12(a) (bright red dots), obtained by tunneling between the superconducting tip and the bare Cu(111) surface, shows a clear quasiparticle gap. In order to obtain the gap value, a least-squares analysis of the data is performed based on a convolution [5] of a constant density of states (DOS) of the Cu sample, including modulation voltage and temperature broadening described by the Fermi–Dirac distribution $f(E) = (1 + \exp[\epsilon/k_B T])^{-1}$, with the quasiparticle excitations ρ_t in the tip:

$$\frac{\partial I_T}{\partial V_T}(E) \propto \int_{-\infty}^{\infty} \rho_t(\epsilon) f'(E-\epsilon)\, \mathrm{d}\epsilon \qquad (14)$$

where the superconducting quasiparticle excitations are given by

$$\rho_t(E) = \mathrm{Re}\left[\frac{E - \mathrm{i}\delta}{\sqrt{(E-\mathrm{i}\delta)^2 - \Delta^2}}\right], \qquad (15)$$

and $f'(E) = \partial f(E)/\partial E$ is the derivative of the Fermi–Dirac distribution. Here, a small imaginary part $\mathrm{i}\delta$ is added to the energy in equation (15) to account for the finite lifetime of the quasiparticles at the gap edge [98].

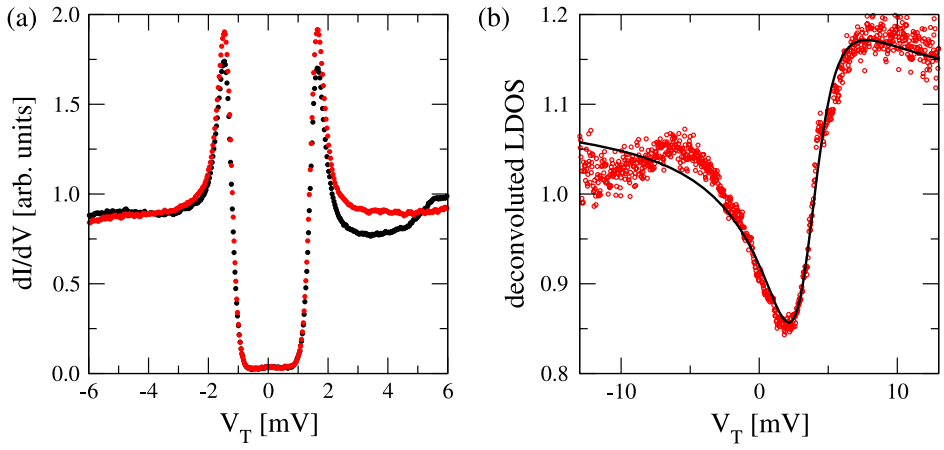

Figure 12. (a) Spectra of the Nb tip measured on the bare Cu(111) surface (bright red dots) and on top of an adsorbed Co adatom (dark black dots) at $T = 0.6$ K, $I_T = 3$ nA and $V_{mod} = 71$ μV. (b) After deconvolution an asymmetric dip is detected in the spectrum (dots) which was successfully fitted with the Fano function using the parameters $q = 0.60$, $E_K = 4.7$ meV and $\Gamma = 2.8$ meV in good agreement with [40, 35].

This analysis yields a gap of width $\Delta = 1.27$ meV. When the same tip is positioned above an isolated Co adatom, the spectrum shown in figure 12(a) (dark black dots) reveals an asymmetry as well as a change of the LDOS in the quasiparticle spectrum at $eV > E_F + \Delta$. However, no impurity-induced gap states are detected.

In order to extract the LDOS of Co/Cu(111) from these spectra, we performed a deconvolution on the basis of

$$\frac{\partial I_T}{\partial V_T}(E) \propto \int_{-\infty}^{\infty} d\epsilon \left[\rho_t(\epsilon)\rho'(E-\epsilon)\big[f(E-\epsilon) - f(\epsilon)\big] - \rho_t(\epsilon)\rho(E-\epsilon)f'(E-\epsilon)\right] \quad (16)$$

using the results of the fit to the BCS-like spectrum and the Co/Cu(111) spectrum obtained with the Nb tip (dark black dots in figure 12(a)). The outcome, depicted in figure 12(b) (dots), shows an asymmetric dip around E_F. A least-squares analysis (line) with the Fano profile (equation (3)) yields a form factor of $q = 0.60$ and a Kondo temperature of $T_K = 32 \pm 5$ K, which is slightly lower than found in previous measurements [40, 35]. The overall shape of the spectrum agrees well with the one shown in figure 6 and with the literature.

Similar results were obtained for all tunneling currents in the range of $I_T = 50$ pA to $I_T = 30$ nA (i.e. 670 kΩ $\leqslant R_T \leqslant$ 400 MΩ). Differential conductance spectra at higher currents corresponding to smaller tip–sample distances could not be obtained owing to tip-induced motions of the Co adatom [75, 81]. Within these limits, no reduction of the superconducting gap width was detected.

In contrast to previous measurements on Mn trimers on Ag(100) [95], the magnetic moment of a single Co adatom hosted on a Cu(111) surface does not induce gap states in a superconducting tip. This is most probably a consequence of effective conduction electron screening of the magnetic moment of the Co adatom on the host metal, as manifested by the observed Kondo resonance. Thus, the superconducting properties of the weakly coupled tip are not affected by the presence of the atomic moment of the impurity on the surface. These differential conductance spectra provide a convincing demonstration for the importance of the convolution of tip and sample density of states [99, 100], a fact often neglected in STS. In the present case, the Kondo resonance on a normal metal surface embosses the quasiparticle density of states of a superconducting tip.

5. Impurity-induced midgap states inside a superconducting energy gap

Interactions between the magnetic moment of a single atom and the superconducting phase are expected. They were detected in spectra probed with normal conducting tips taken on top of adatoms hosted on a Nb sample, which is a classical superconductor [94], on top of Zn impurities on a high-T_C superconductor [101], and in experiments on Cr and Co atoms adsorbed on a superconducting Pb film on Si probed by a superconducting Nb tip [102]. We note for the latter experiment that the midgap states found in these superconductor–insulator–superconductor junctions are not the signature of Andreev reflections between superconductors with different gap energies, as Andreev reflections are only observed at much lower tunneling resistance [103].

Here we present first results of a similar experiment using a superconducting tip. A single Co atom was attached to the tip apex by using atomic manipulation techniques [75]. These measurements are basically mirror experiments of the work of Yazdani *et al* [94].

Figure 13(a) shows a dI/dV spectrum of a superconducting Nb tip with a single Co atom on its the apex obtained by tunneling to a clean Cu(111) surface at a base temperature of $T = 0.6$ K. While in the previous measurements [94] the subgap peak structure was only observable after subtraction of the unperturbed BCS-like spectrum of the tip from the measured data, the spectrum of figure 13(a) reveals clearly detectable midgap states directly in the dI/dV curves without further data treatment. Furthermore, the quasiparticle gap is reduced to $\Delta = 1.15$ meV, as compared to the one measured without a cobalt atom on its apex, where a value of $\Delta = 1.27$ meV was

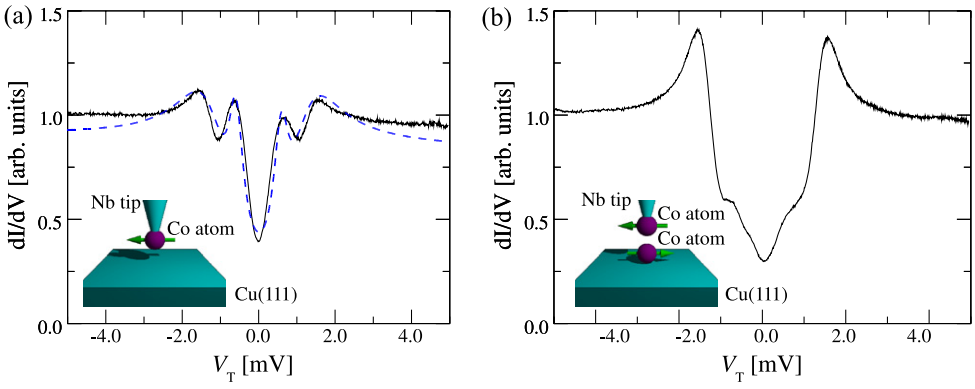

Figure 13. Tunneling spectra taken at a temperature of $T = 0.5$ K in a tunneling junction consisting of a Co atom attached to the tip apex of a superconducting Nb tip above a bare Cu(111) single-crystal surface (a). The dashed line (blue) is the calculated spectrum using a model describing a classical spin on a superconductor [104, 105]. The intensity of the midgap states are drastically reduced when the Co/Nb tip is placed over a second Co atom which is adsorbed on the Cu(111) surface (b). Tunneling parameters: $V_T = -5$ mV, $I_T = 1$ nA, $V_{mod} = 71$ μV.

obtained (see figure 12(a)). This is a clear sign of the pair-breaking effect of the magnetic impurity on the superconducting state.

We can assign the symmetrical appearance of the midgap peaks at an energy of $\epsilon_{1,2} \approx \pm 0.60$ meV to two spin-polarized states. While the singlet state of the superconductor is only weakly influenced by a pure Coulomb scattering potential [106] a magnetic moment $w = \frac{1}{2}JS$, with S as the local impurity spin and J as the exchange coupling, has a strong pair-breaking effect and induces the observed bound states inside the quasiparticle gap [107, 108, 104, 105].

The scattering of a Cooper pair on the impurity can be characterized by introducing a spin-mixing angle Θ which is a phenomenological parameter describing the degree of 'spin-mixing' of the quasiparticle spins of the superconducting state induced by the magnetic adatom [109]. Within this description, the position of the midgap states is given by

$$\epsilon_{1,2} = \pm\Delta \cos\left(\frac{\Theta}{2}\right), \tag{17}$$

leading to a spin-mixing of $\Theta \approx \frac{2}{3}\pi$ for the data presented in figure 13(a).

The magnetic exchange interaction w between the impurity and the Cooper pairs of the host Nb sample and the on-site Coulomb potential U can be extracted by analyzing the position and amplitude of the peaks [104, 105]. We found that $\pi N_F w = 0.56$ and $\pi N_F U = 0.069$ (with N_F as the density of states at E_F in the normal phase) reproduces the obtained data sufficiently as depicted in figure 13(a) (dashed line). The small but non-vanishing Coulomb potential is at the origin of the particle–hole asymmetry observed in the data as different peak amplitudes.

There exists another interesting result: using the same tip with the attached Co atom to measure the dI/dV spectrum on top of a *second* single Co adatom supported on the Cu(111) surface reveals strongly suppressed midgap states (see figure 13(b)).

This result is surprising considering the obtained spectrum of Co on Cu(111) using a *clean* superconducting Nb tip in which the Kondo resonance was clearly detected (see figure 12(a)). The reduced intensity of the midgap states, as well as the stronger characteristics of the BCS gap which almost displays its undisturbed shape, can be understood by assuming similar spin-polarized states in the sample as well as in the apex of the tip and an *antiferromagnetic* coupling between the two Co adatoms [105]. This coupling must be strong enough to destroy the Kondo screening on the normal conducting surface. Temperature-dependent measurements which have not yet been performed would reveal how this coupling changes when the tip reaches the critical temperature and loses its superconducting properties.

These experiments indicate an interesting path to create magnetic systems with long spin lifetimes. The spin-relaxation time is extended due to the decoupling from the environment by the absence of electronic states in the superconducting gap. Interactions can be further reduced by choosing a superconductor without nuclear spin so that the dipole–dipole interaction between the impurity and the nuclear moment does not play a role in the spin relaxation [105].

6. 3d transition metal atoms on ultrathin dielectric films

We have seen in section 1 that the local density of states of the local environment of the Kondo impurity plays a decisive role for the actual Kondo temperature the system acquires and for the shape of the detected resonance around the Fermi energy. For example, for Co–, Fe–and Mn–phthalocyanine molecules supported on metal surfaces, the decoupling from the supporting surface leads to Kondo peaks [46–48] instead of Kondo dips. Such Kondo peaks have also been reported for Co clusters supported on a carbon nanotube [110]. It was therefore tempting to investigate more generally adatom–substrate systems where the magnetic adatom is deliberately decoupled from the metallic substrate by an ultrathin dielectric film.

First STS results have been obtained for single manganese adatoms positioned on a NiAl(110) alloy surface and on an ultrathin Al_2O_3 layer on NiAl(110) [66]. On the metallic

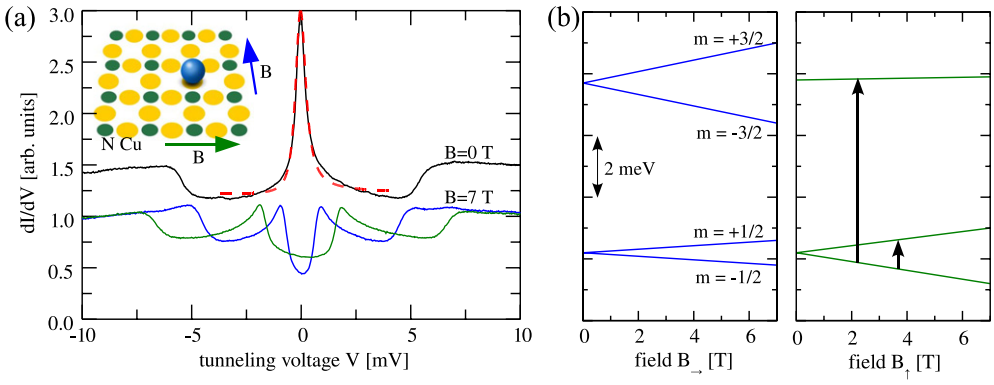

Figure 14. (a) Spectra of a Co atom on CuN/Cu(100) measured at a temperature of $T = 0.5$ K and an external magnetic field of $B = 0$ and 7 T. The zero-field spectrum reveals a Kondo peak which is fitted to a temperature-broadened Fano function (red dashed line) and IETS steps at $V \approx \pm 6$ mV due to $m = \pm 1/2 \rightarrow m = \pm 3/2$ spin-flip transitions [15]. At $B = 7$ T, the spin-flip step positions have moved and the Kondo peak has split. This splitting depends strongly on the direction of the magnetic field. Inset: schematic of the CuN surface, the adsorption position of the Co adatom (on top of a Cu atom) and the field directions (colored arrows). (b) Energy eigenlevels for different magnetic fields and directions. The arrows indicate exemplary possible spin transitions with $\Delta m = \pm 1$ or 0.

substrate no significant spectral feature around E_F is observed, pointing to strong coupling and charge transfer between the magnetic adatom and the conduction electrons of the metallic substrate which inhibits the Kondo effect or displaces it to an energy range outside the experimental energy window. These results change for impurities on the Al_2O_3 surface close to a metal–oxide interface step. Here a well-developed peak at E_F with a Kondo temperature between 3 and 6 K and a relatively large Fano parameter q has been detected. Evidently, the coupling between the magnetic adatom and the metallic host is still strong enough to allow for Kondo scattering, but the dielectric spacer layer inhibits sufficiently the direct tunneling path to the metallic substrate, resulting in a Kondo peak in the spectroscopic measurement. However, for manganese atoms on the oxide layer at a further distance from the metal–oxide interface step no Kondo peak was observed, presumably due to a further reduction of the hybridization with bulk states which lowered the Kondo temperature below the detection limit of the experimental set-up operating at a temperature of 0.5 K. These results clearly show the crucial dependence of the Kondo effect on the local environment of the magnetic adatoms.

We note that, in general, a decoupling of adsorbed atomic or molecular species from a metallic substrate by dielectric spacer layers enables the study of the physical properties of the adatom or adsorbed molecule. Examples are the detection of STM-induced light emission from molecules supported on ultrathin dielectric films on metals (Al_2O_3 on NiAl(110) [111] and NaCl on Au(111) [112]) and, taking advantage of another type of inelastic electron tunneling spectroscopy (IETS), the study of the magnetic properties of single magnetic adatoms [66] and of one-dimensional atomic chains engineered with the tip of an STM [113] on a CuN layer on Cu(100) [114].

7. The interplay between magnetic anisotropy and Kondo effect

Magnetic adatoms are strongly influenced by the surrounding or supporting crystal environment, giving rise to magnetocrystalline anisotropy, which describes the dependence of the total energy on the direction of the spin. The STM is able to measure this anisotropy by means of the spin-excitation spectrum at different magnetic fields [84]. The analysis of these spin-flip excitation spectra, where the spin excitation leads to characteristic steps in the differential conductance (dI/dV) spectra indicative of the opening of a new conductance channel, led to the discovery of the large magnetic anisotropy of the spin of individual iron atoms embedded in the surface molecular network of CuN [84].

These results paved the way for the next logical step in the investigation of the interactions of single magnetic adatoms with the conduction electrons of the support: the study of systems where the many-body Kondo effect and the magnetic anisotropy, usually described within a single-particle approximation, are of similar strength. The system chosen was cobalt on a decoupling layer of CuN on Cu(100) [15].

Figure 14(a) shows spectra of a cobalt atom on CuN/Cu(100) at zero magnetic field B and at $B = 7$ T. The cobalt adatom is located in a stable atop position on a copper atom in the CuN surface plane. The external magnetic field is applied either parallel to the nearest-neighbor hollow sites or perpendicular to this direction along the two nearest nitrogen neighbors of the cobalt adatom, as illustrated in the inset of figure 14(a). The zero-field spectrum reveals a prominent Kondo peak close to E_F which has a Kondo temperature of $T_K = 2.6 \pm 0.2$ K. This is substantially lower than the value of 54 K reported for cobalt atoms in direct contact with a Cu(100) surface [35]. In addition to the Kondo peak, prominent steps at $V = \pm 6.2$ mV are observed which are due to inelastic spin-flip tunneling.

At an applied magnetic field of $B = 7$ T, the spin-flip excitation step positions shift differently and the Kondo peak splits differently, depending on the magnetic field direction with respect to the two indicated high-symmetry crystallographic directions. We note that Zeeman splitting of a Kondo resonance in an external magnetic field has been observed before in STS for Mn on Al_2O_3

on NiAl(110) [66], for Mn–phthalocyanine molecules on Pb islands on Si(111) [48] and in previous studies of quantum dots [27, 13], in single-atom transistors [115], in single-molecule transistors [116], in zero-bias tunneling anomalies (planar tunnel junctions) [117] and in single-electron transistors [83]. In the present case, however, the rate at which the field splits depends strongly on the direction of the applied external magnetic field B. This directional dependence of the Kondo peak splitting is indicative of the presence of a strong magnetocrystalline anisotropy.

The spectra can be rationalized within a single-electron Hamiltonian which accounts for the Zeeman energy and for an uniaxial anisotropy energy [15]:

$$\hat{H} = -g\mu_B \mathbf{B}\hat{\mathbf{S}} + D\hat{S}_z^2, \tag{18}$$

with the Landé factor g and the Bohr magneton μ_B.

The anisotropy parameter D in this equation partly breaks the zero-field degeneracy of the eigenlevels of a spin system with a total spin $S > 1/2$. A free cobalt atom with the electronic configuration [Ar] $3d^7 4s^2$ has a total spin of $S = 3/2$ according to Hund's rule. Using the same spin value for the cobalt atom on top of the CuN together with $g = 2.2$ and $D = 2.75$ meV allows us to explain the observed spectra: The zero-field IETS steps at ± 6 mV are due to $m = \pm 1/2 \rightarrow m = \pm 3/2$ spin-flip transitions whereby m denotes the eigenvalue of the z projection $\hat{S}_z$ of the spin vector $\hat{\mathbf{S}}$ with the quantization axis z along the nitrogen neighbors [15]. We note the crucial observation that the $m = \pm 1/2$ states are degenerate. This allows conduction electrons to spin-flip between these states, leading to the appearance of the Kondo resonance.

When a magnetic field is applied, the energies of the eigenstates change according to equation (18) (see figure 14(b)) and the $m = \pm 1/2$ ground state is no longer degenerate. This results in additional IETS steps due to the $m = -1/2 \rightarrow m = +1/2$ transition. Furthermore, the Kondo peak splits precisely following the calculated low-energy transition of the non-Kondo Hamiltonian of equation (18).

From the quantitative analysis of the evolution of the Kondo peak splitting and of the higher-lying spin-flip excitations as a function of the applied magnetic field we conclude that Kondo screening for adatoms with a spin larger than $S = 1/2$ is different from the one of simple $S = 1/2$ Kondo systems, because a spin $S > 1/2$ is sensitive to the influence of the magnetocrystalline anisotropy, leading to different energies for different spin orientations. Kondo screening for these systems can only occur if the anisotropy results in degenerate or almost degenerate ground state levels (compared to the characteristic Kondo energy $k_B T_K$) connected by $\Delta m = 1$ transitions [15]. We note these experimental results are in agreement with recent theoretical calculations of spin systems in anisotropic environments [118, 119].

The Kondo resonance is not only characterized by the splitting in an external magnetic field but also by a characteristic temperature dependence. Figure 15 shows a rapid reduction of the Kondo peak height with increasing sample temperature for the system Co on CuN [15]. The intrinsic temperature dependence of the resonance width Γ, has been obtained after deconvolution of the thermal broadening described by the Fermi–Dirac distribution of the tunneling electrons in the tip (see equation (14)) and is shown in the inset of the figure.

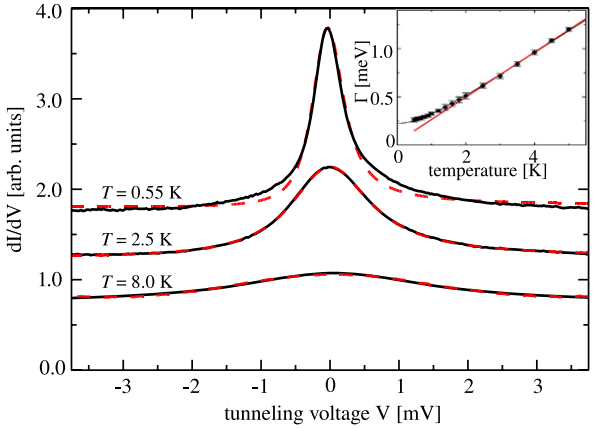

Figure 15. The Kondo peak of a Co atom on CuN/Cu(100) measured at different sample temperatures (black lines) and fits to a temperature-broadened Fano function (red dashed lines) Inset: intrinsic half-width Γ extracted from the fits. The red line shows the linear behavior of Γ at high temperature and has a slope of $(5.4 \pm 0.1)k_B$ [15].

As expected, the intrinsic width grows linearly with temperature for higher temperatures whereas it saturates at a finite value at low temperature. The coefficient of the linear slope of $5.4k_B$ is consistent with earlier temperature-dependent measurements on Kondo systems where a high-temperature broadening proportional to $4.5k_B T$ in quantum dots [13] and $\approx 5k_B T$ on individual Ti atoms on Cu(100) was found [14]. These data are in excellent agreement with the Fermi liquid model which predicts a slope $\alpha = 5.4k_B$ [11].

We note that this temperature dependence is a clear and unique signature of the Kondo effect. Other processes such as, for example, inelastic spin-flip transitions which are also found in the Co/CuN system (figure 14) or vibrational excitations do not broaden with the same ratio. For these processes only *one* state, the final or initial state, lies in the sample and is influenced by the Fermi–Dirac broadening of the sample temperature leading to a temperature-dependent width of $3.2k_B T$ (see process no. (3) in figure 2(c)), while the initial *and* final state of the Kondo scattering process are located in the sample and thus broadened by the sample temperature (see figure 2(b)).

8. Interactions between magnetic adatoms

If there are several magnetic impurities on a surface, modifications of the Kondo resonance of the individual adatoms due to magnetic interactions are expected. Depending on their mutual lateral distance on the surface and on the coupling strength with the supporting substrate, magnetic dipolar coupling, direct exchange due to overlap of the localized impurity orbitals or indirect exchange interaction via the host conduction electrons, the Ruderman–Kittel–Kasuya–Yosida (RKKY) interaction [120–123] may be active. For three

dimensions, this RKKY exchange coupling j for a magnetic impurity at the origin in a free-electron gas decays with distance r in an oscillatory manner as $j(r) \propto \cos(2k_F r)/r^3$, where k_F denotes the Fermi wavevector. For two dimensions, $j(r)$ decays with $1/r^2$ [124]. Therefore, a second magnetic impurity, depending on its distance from the first impurity, will couple antiferromagnetically or ferromagnetically to the first one via the conduction electrons of the supporting host.

The first experiment on an atomic scale to monitor such modifications of the Kondo resonance reported on the disappearance of the Kondo resonance for a cobalt dimer at small interatomic distances [125]. Using STS and atomic manipulation to study the interaction between a single pair of Co atoms at the surface of nonmagnetic Au, the local electronic structure of the Co adatoms was measured for different Co–Co spacings at $T = 6$ K. Co dimers, created by manipulation with the STM tip, were found to show an abrupt disappearance of the Kondo resonance for Co separations of less than 0.6 nm. This behavior was explained as the result of reduced exchange coupling between Au conduction electrons and ferromagnetic Co dimers [125].

In a subsequent experiment the Kondo response of a single antiferromagnetic trimer was investigated [126]. The authors used atomic manipulation and STS to probe the local behavior of a triangular chromium trimer on Au(111). The chromium trimers could be reversibly switched between two distinct electronic states, one where a Kondo resonance was present, and a second one where the Kondo resonance was absent. This phenomenon was explained as the Kondo response of a spin-switching, magnetically frustrated nanocluster, consistent with noncollinear magnetic states predicted for chromium trimers whose structures differ by the position of a single atom.

Motivated by these results, the evolution of the Kondo lineshape obtained by STS has been studied again by varying the interatomic distance between cobalt adatoms in dimer and trimer configurations on a Cu(100) single-crystal surface. The results have been analyzed within many-body theory in order to determine the magnetic coupling as a function of the interatomic spacing [127]. As lateral manipulation of atoms on (100) metal surfaces is hindered by a high-energy barrier between neighboring surface sites, dimers with well-defined interatomic distances have been created with a different approach. First, cobalt carbonyl complexes are formed [44], in which the CO ligands inhibit nucleation and island formation and facilitate the growth of one-dimensional structures. Subsequently, the CO ligands have been removed by tip-induced dissociation of the molecules. Different cobalt dimer configurations have been prepared with interatomic distances between the neighboring cobalt atoms ranging from 0.256 to 0.81 nm. For cobalt dimers with interatomic cobalt distances smaller than 0.5 nm these experiments confirmed the observations of the disappearance of the Kondo resonance [125]. However, for an interatomic cobalt distance of 0.512 nm the authors observed a clear broadening of the Kondo resonance as compared to the one found for a single cobalt atom. They interpreted this broadening as the manifestation of sufficiently strong antiferromagnetic coupling leading to a splitting of the Kondo resonance (not resolved in the experimental spectrum) and to the formation of a singlet state between the two cobalt impurities. Using many-body theory, the authors were able to follow the oscillatory transition (RKKY) from ferromagnetic through antiferromagnetic back to ferromagnetic coupling. Adding a third atom to the antiferromagnetically coupled dimer resulted in the formation of a collective correlated state [127].

In a recent theoretical study, the magnetic properties of subnanometer structures have been tuned by adjusting the geometry of the system [128]. The authors demonstrate that the magnetic moment of a single adatom coupled to a buried magnetic cobalt layer can be stabilized in either a ferromagnetic or an antiferromagnetic configuration, depending on the copper spacer thickness owing to quantum confinement. It is found that a buried cobalt layer has a profound effect on the exchange interaction between two magnetic impurities on the surface. Moreover the authors calculate that the exchange interaction between magnetic adatoms on a surface can be manipulated by introducing nonmagnetic Cu chains to link them [128]. Here it is interesting to note that the system of Co adatoms on Cu multilayers on a buried Co layer has been studied experimentally at the same time [49]. In contrast to the theoretical prediction of stable ferromagnetic or antiferromagnetic Co adatoms, the authors of the experiment found quantum-well state-induced modulations of the Kondo resonance, i.e. dynamic spin-flip processes and not a stable magnetic moment.

In order to investigate the consequences of direct coupling between a ferromagnetic Co surface and single magnetic Fe and Co adatoms, STS with a spin-polarized Cr tip has been used and the results have been compared to first-principles calculations. These magnetic adatoms have been found to exhibit stationary out-of-plane spin polarization, but have opposite sign of the exchange coupling between electron states of the adatom and the Co island surface state: Fe adatoms exhibit parallel spin polarization to the Co surface state while Cr adatoms exhibit antiparallel spin polarization [129].

In a related experiment, using STS with a spin-polarized tip, the oscillating indirect exchange interactions between individual Co adatoms at different lateral distances to a Co nanowire on a nonmagnetic Pt(111) substrate have been observed for the first time [130]. The decay of the RKKY function with distance from the Co nanowire was found to be close to $j(r) \propto \cos(2k_F r)/r$, which is expected if the interaction is dominated by 2D states and the superposition of the contributions from all Co atoms along the stripe edge (nanowire) attenuates the decay. In this way the variations of the magnetic properties of identical Co adatoms were found to be due to different local environments.

Furthermore, experiments have been carried out in which Kondo systems in quantum dots [131] or electromigration junctions [132] have shown remarkable changes in their properties through spin–spin coupling with either a second quantum dot or magnetic impurities in the connecting leads.

Very recently, similar experiments have been performed by coupling individual magnetic atoms with a Kondo impurity [133]. In these experiments the atoms are decoupled

from the supporting metal substrate by an ultrathin dielectric film of CuN. The spin coupling between the atoms is provided mainly by the nitrogen atoms of the CuN network, enabling us to adjust the coupling strength by choosing proper adsorption sites either along the nitrogen rows or perpendicular to them (see also the inset of figure 14(a)). While it was found that chains of nearest-neighboring Mn atoms along the nitrogen direction are antiferromagnetically coupled via Heisenberg interactions and act for rows up to 10 Mn atoms like a single quantum object in which the spectroscopic signature shows only slight variations along the chain [113], the atoms in the new experiments show a different behavior. Different pairs of Co, Fe and Mn atoms were positioned at a distance of 0.72 nm perpendicular to the nitrogen rows so that they are relatively weakly coupled. The atoms of these pairs show the characteristic spin-flip IET steps and Kondo features of the individual atoms [84, 15] but slightly distorted by the neighboring magnetic atom. For example, the Kondo peak of a Co atom is already split in a Co–Fe pair at zero magnetic field and can be restored by applying an appropriate magnetic field [133]. The author was able to describe the system of coupled atoms quantitatively within a Hamiltonian accounting for the individual Zeeman energy, the anisotropy energy and a spin–spin exchange term.

9. Outlook

Both experiment and theory of Kondo systems have made considerable progress during the last few years. Low-temperature STS at 0.5 K in ultra-high vacuum with atomic-scale spatial and down to 10 μeV energy resolution, together with its lateral and vertical atom manipulation capabilities, opened new insights into the interplay between Kondo physics, magnetic anisotropy, localized spin-flip excitations and the magnetic exchange interaction. With these experimental and theoretical tools the study of collective Kondo states, e.g. Kondo lattices or heavy-fermion systems, will become accessible. The interaction of magnetic atoms with superconducting materials will be one of the next challenging steps at even lower temperatures down to the mK region. The Cooper pairs of the superconductor are scattered at impurity sites, resulting in spin-selective states inside the superconducting gap even without an external magnetic field. Thus, a superconducting tip with a magnetic atom on its apex allows us to measure spin-selective tunneling currents with minimal stray fields. The interaction of magnetic atoms which have their spin excitations energies inside the superconducting gap are candidates for systems with long spin lifetime. Such investigations may lead to interesting applications in spintronic and quantum computing.

Acknowledgments

The authors would like to thank C F Hirjibehedin, C P Lutz, A F Otte, K v Bergmann, S Loth, H Brune, B A Jones, D M Eigler, J Kroha, F Patthey and M Pivetta for stimulating discussions and for a very fruitful collaboration. MT and WDS would like to acknowledge financial support by the Swiss National Science Foundation. MT and AJH would like to acknowledge financial support by the Office of Naval Research. WDS would like to acknowledge the outstanding hospitality of the Stiftung Dr. Robert und Lina Thyll-Dürr (Switzerland): 2008-Arbeitsaufenthalt in der Casa Zia Lina, Elba, als Gast der Stiftung Dr Robert und Lina Thyll-Dürr (Schweiz).

References

[1] Meissner W and Voigt B 1930 Messungen mit Hilfe von flüssigem Helium XI Widerstand der reinen Metalle in tiefen Temperaturen *Ann. Phys., Lpz.* **7** 761
[2] de Haas W J, de Boer J and van dën Berg G J 1934 The electrical resistance of gold, copper and lead at low temperatures *Physica* **34** 1115
[3] Kondo J 1964 Resistance minimum in dilute magnetic alloys *Prog. Theor. Phys.* **32** 37
[4] Kondo J 1968 Effect of ordinary scattering on exchange scattering from magnetic impurity in metals *Phys. Rev.* **169** 437
[5] Ternes M 2006 Scanning tunneling spectroscopy at the single atom scale *PhD Thesis* École Polytechnique Fédérale de Lausanne http://library.epfl.ch/en/theses/?nr=3465
[6] Anderson P W 1961 Localized magnetic states in metals *Phys. Rev.* **124** 41
[7] Plihal M and Gadzuk J W 2001 Nonequilibrium theory of scanning tunneling spectroscopy via adsorbate resonances: Nonmagnetic and Kondo impurities *Phys. Rev.* B **63** 085404
[8] Kouwenhoven L and Glazman L 2001 Revival of the Kondo effect *Phys. World* **14** (January) 33
[9] Újsághy O, Kroha J, Szunyogh L and Zawadowski A 2000 Theory of the Fano resonance in the STM tunneling density of states due to a single Kondo impurity *Phys. Rev. Lett.* **85** 2557
[10] Hewson A C 1997 *The Kondo Problem to Heavy Fermions* (Cambridge: Cambridge University Press)
[11] Nozières P 1974 A Fermi-liquid description of the Kondo problem at low temperatures *J. Low Temp. Phys.* **17** 31
[12] Costi T A, Hewson A C and Zlatic V 1994 Transport coefficients of the Anderson model via the numerical renormalization group *J. Phys.: Condens. Matter* **6** 2519
[13] Cronenwett S M, Oosterkamp T H and Kouwenhoven L P 1998 A tunable Kondo effect in quantum dots *Science* **281** 540
[14] Nagaoka K, Jamneala T, Grobis M and Crommie M F 2002 Temperature dependence of a single Kondo impurity *Phys. Rev. Lett.* **88** 077205
[15] Otte A F, Ternes M, Loth S, von Bergmann K, Brune H, Lutz C P, Hirjibehedin C F and Heinrich A J 2008 The role of magnetic anisotropy in the Kondo effect *Nat. Phys.* **4** 847
[16] Lambe J and Jaklevic R C 1968 Molecular vibration spectra by inelastic electron tunneling *Phys. Rev.* **165** 821
[17] Patthey F, Delley B, Schneider W-D and Baer Y 1985 Low-energy excitations in α- and γ-Ce observed by photoemission *Phys. Rev. Lett.* **55** 1518
[18] Patthey F, Schneider W-D, Baer Y and Delley B 1987 High-temperature collapse of the Kondo resonance in $CeSi_2$ observed by photoemission *Phys. Rev. Lett.* **58** 2810
[19] Patthey F, Imer J-M, Schneider W-D, Beck H, Baer Y and Delley B 1990 High-resolution photoemission study of the low-energy excitations in 4f-electron system *Phys. Rev.* B **42** 8864
[20] Laubschat C, Weschke E, Holtz C, Domke M, Strebel O and Kaindl G 1990 Surface electronic structure of α-like Ce compounds *Phys. Rev. Lett.* **65** 1639

[21] Weschke E, Laubschat C, Simmons T, Domke M, Strebel O and Kaindl G 1991 Surface and bulk electronic structure of Ce metal studied by high-resolution resonant photoemission *Phys. Rev.* B **44** 8304

[22] Ehm D, Hüfner S, Reinert F, Kroha J, Wölfle P, Stockert O, Geibel C and Löhneysen H v 2007 High-resolution photoemission study on low-T_K Ce systems: Kondo resonance, crystal field structures, and their temperature dependence *Phys. Rev.* B **76** 045117

[23] Wuilloud E, Moser H R, Schneider W-D and Baer Y 1983 Electronic structure of γ and α-Ce *Phys. Rev.* B **28** 7354

[24] Gschneidner K A and Eyring L 1987 *Handbook on the Physics and Chemistry of the Rare Earths* (Amsterdam: North-Holland)

[25] Li J T, Schneider W-D, Berndt R and Delley B 1998 Kondo scattering observed at a single magnetic impurity *Phys. Rev. Lett.* **80** 2893

[26] Madhavan V, Chen W, Jamneala T, Crommie M F and Wingreen N S 1998 Tunneling into a single magnetic atom: spectroscopic evidence of the Kondo resonance *Science* **280** 567

[27] Goldhaber-Gordon D, Shtrikman H, Mahalu D, Abusch-Magder D, Meirav U and Kastner M A 1998 Kondo effect in a single-electron transistor *Nature* **391** 156

[28] Schneider W-D 1999 A local view of the Kondo effect: scanning tunneling spectroscopy *Pramana J. Phys.* **52** 537

[29] Schneider W-D and Berndt R 2000 Low-temperature scanning tunneling spectroscopy: Kondo effect and surface state lifetimes *J. Electron Spectrosc. Relat. Phenom.* **109** 19

[30] Schneider W-D 2004 Low-temperature scanning tunneling microscopy *Encyclopedia of Nanoscience and Nanotechnology* vol 4 ed H S Nalwa (Valencia, CA: American Scientific) pp 667–88

[31] Néel N, Kröger J, Limot L, Palotás K, Hofer W A and Berndt R 2007 Conductance and Kondo effect of a controlled single atom contact *Phys. Rev. Lett.* **98** 016801

[32] Fano U 1961 Effects of configuration interaction on intensities and phase shifts *Phys. Rev.* **124** 1866

[33] Harmon B N and Freeman A J 1974 Spin-polarized energy-band structure, conduction-electron polarization, spin densities, and the neutron magnetic form factor of ferromagnetic gadolinium *Phys. Rev.* B **10** 1979

[34] Lang N D 1986 Spectroscopy of single atoms in the scanning tunneling microscope *Phys. Rev.* B **34** 5947

[35] Knorr N, Schneider M A, Diekhöner L, Wahl P and Kern K 2002 Kondo effect of single Co adatoms on Cu surfaces *Phys. Rev. Lett.* **88** 096804

[36] Schneider M A, Vitali L, Knorr N and Kern K 2002 Observing the scattering phase shift of isolated Kondo impurities at surfaces *Phys. Rev.* B **65** 121406

[37] Wahl P, Diekhöner L, Schneider M A, Vitali L, Wittich G and Kern K 2004 Kondo temperature of magnetic impurities at surfaces *Phys. Rev. Lett.* **93** 176603

[38] Limot L and Berndt R 2004 Kondo effect and surface-state electrons *Appl. Surf. Sci.* **237** 576

[39] Henzl J and Morgenstern K 2007 Contribution of the surface state to the observation of the surface Kondo resonance *Phys. Rev. Lett.* **98** 266601

[40] Manoharan H C, Lutz C P and Eigler D M 2000 Quantum mirages formed by coherent projection of electronic structure *Nature* **403** 512

[41] Quaas N 2003 Scanning tunnelling microscopy of co-impuried noble metal surfaces: Kondo-effect, electronic surface states and diffusive atom transport *PhD Thesis* University of Göttingen

[42] Quaas N, Wenderoth M, Weismann A and Ulbrich R G 2004 Kondo resonance of single Co atoms embedded in Cu(111) *Phys. Rev.* B **69** 201103

[43] Tournier R and Blandin A 1970 Influence of interactions between impurities on the appearance of magnetic moments in copper–cobalt dilute alloys *Phys. Rev. Lett.* **24** 397

[44] Wahl P, Diekhöner L, Wittich G, Vitali L, Schneider M A and Kern K 2005 Kondo effect of molecular complexes at surfaces: ligand control of the local spin coupling *Phys. Rev. Lett.* **95** 166601

[45] Néel N, Kröger J, Berndt R, Wehling T, Lichtenstein A and Katsnelson M I 2008 Controlling the Kondo effect in $CoCu_n$ clusters atom by atom arXiv:0810.0236 [cond-mat]

[46] Zhao A *et al* 2005 Controlling the Kondo effect of an adsorbed magnetic ion through its chemical bonding *Science* **309** 1542

[47] Gao L *et al* 2007 Site-specific Kondo effect at ambient temperatures in iron-based molecules *Phys. Rev. Lett.* **99** 106402

[48] Fu Y-S *et al* 2007 Manipulating the Kondo resonance through quantum size effects *Phys. Rev. Lett.* **99** 256601

[49] Uchihashi T, Zhang J, Kröger J and Berndt R 2008 Quantum modulation of the Kondo resonance of Co adatoms on Cu/Co/Cu(100): low-temperature scanning tunneling spectroscopy study *Phys. Rev.* B **78** 033402

[50] Luo H G, Xiang T, Wang X Q, Su Z B and Yu L 2004 Fano resonance for anderson impurity systems *Phys. Rev. Lett.* **92** 256602

[51] Kolf Ch, Kroha J, Ternes M and Schneider W-D 2006 Comment on Fano resonance for Anderson impurity systems *Phys. Rev. Lett.* **96** 019701

[52] Luo H G, Xiang T, Wang X Q, Su Z B and Yu L 2006 Reply to comment on 'Fano resonance for Anderson impurity systems' *Phys. Rev. Lett.* **96** 019702

[53] Jamneala T, Madhavan V, Chen W and Crommie M F 2000 Scanning tunneling spectroscopy of transition-metal impurities at the surface of gold *Phys. Rev.* B **61** 9990

[54] Kroha J 2005 private communication

[55] Affleck I and Simon P 2001 Detecting the Kondo screening cloud around a quantum dot *Phys. Rev. Lett.* **86** 2854

[56] Affleck I, Borda L and Saleur H 2008 Friedel oscillations and the Kondo screening cloud *Phys. Rev.* B **77** 180404

[57] Bergmann G 2008 Quantitative calculation of the spatial extension of the Kondo cloud *Phys. Rev.* B **77** 104401

[58] Ashcroft N W and Mermin N D 1976 *Solid State Physics* (Philadelphia: Holt Rinehart and Winston)

[59] Silly F, Pivetta M, Ternes M, Patthey F, Pelz J P and Schneider W-D 2004 Creation of an atomic superlattice by immersing metallic adatoms in a two-dimensional electron sea *Phys. Rev. Lett.* **92** 016101

[60] Silly F, Pivetta M, Ternes M, Patthey F, Pelz J P and Schneider W-D 2004 Coverage-dependent self-organization: from individual adatoms to adatom superlattices *New J. Phys.* **6** 16

[61] Ternes M, Weber C, Pivetta M, Patthey F, Pelz J P, Giamarchi T, Mila F and Schneider W-D 2004 Scanning-tunneling spectroscopy of surface-state electrons scattered by a slightly disordered two-dimensional dilute 'solid': Ce on Ag(111) *Phys. Rev. Lett.* **93** 146805

[62] Stassis C, Gould T, McMasters O D, Gschneidner K A and Nicklow R M 1979 Lattice and spin dynamics of γ-Ce *Phys. Rev.* B **19** 5746

[63] Liu L Z, Allen J W, Gunnarsson O, Christensen N E and Anderson O K 1992 α–γ transition in Ce: a detailed analysis of electron spectroscopy *Phys. Rev.* B **45** 8934

[64] Franceschi E and Olcese G L 1969 A new allotropic form of cerium due to its transition under pressure to the tetravalent state *Phys. Rev. Lett.* **22** 1299

[65] Galera R M, Givord D, Pierre J, Murani A P, Schweizer J, Vettier C and Ziebeck K R A 1985 Polarized neutron scattering in Kondo or intermediate valence compounds *J. Magn. Magn. Mater.* **52** 103

[66] Heinrich A J, Gupta J A, Lutz C P and Eigler D M 2004 Single-atom spin-flip spectroscopy *Science* **306** 466

[67] Daybell M D and Steyert W A 1968 Localized magnetic impurity states in metals: some experimental relationships *Rev. Mod. Phys.* **40** 380

[68] Gruner G and Zawadowski A 1974 Magnetic impurities in non-magnetic metals *Rep. Prog. Phys.* **37** 1497

[69] Riegel D and Gross K D 1990 Magnetism and electronic structure of 3d and 4d ions in metals *Physica* B **163** 678

[70] Schneider M A, Vitali L, Wahl P, Knorr N, Diekhöner L, Wittich G, Vogelgesang M and Kern K 2005 Kondo state of Co impurities at noble metal surfaces *Appl. Phys.* A **80** 937

[71] Gupta J A, Lutz C P, Heinrich A J and Eigler D M 2005 Strongly coverage-dependent excitations of adsorbed molecular hydrogen *Phys. Rev.* B **71** 115416

[72] Gaudioso J, Lauhon L J and Ho W 2000 Vibrationally mediated negative differential resistance in a single molecule *Phys. Rev. Lett.* **85** 1918

[73] Pivetta M, Ternes M, Patthey F and Schneider W-D 2007 Diatomic molecular switches to enable the observation of very-low-energy vibrations *Phys. Rev. Lett.* **99** 126104

[74] Gaisch R, Gimzewski J K, Reihl B, Schlittler R R, Tschudy M and Schneider W-D 1992 Low-temperature ultra-high-vacuum scanning tunneling microscope *Ultramicroscopy* **42** 1621

[75] Stroscio J A and Eigler D M 1991 Atomic and molecular manipulation with the scanning tunneling microscope *Science* **254** 1319

[76] Bartels L, Meyer G and Rieder K-H 1997 Controlled vertical manipulation of single CO molecules with the scanning tunneling microscope: a route to chemical contrast *Appl. Phys. Lett.* **71** 213

[77] Lauhon L J and Ho W 2000 Direct observation of the quantum tunneling of single hydrogen atoms with a scanning tunneling microscope *Phys. Rev. Lett.* **85** 4566

[78] Fernández-Torres L C, Sykes E C H, Nanayakkara S U and Weiss P S 2006 Dynamics and spectroscopy of hydrogen atoms on Pd(111) *J. Phys. Chem.* B **110** 7380

[79] Lauhon L J and Ho W 2000 Control and characterization of a multistep unimolecular reaction *Phys. Rev. Lett.* **84** 1527

[80] Klein C, Eichler A, Hebenstreit E L D, Pauer G, Koller R, Winkler A, Schidt M and Varga P 2003 When scanning tunneling microscopy gets the wrong adsorption site: H on Rh(100) *Phys. Rev. Lett.* **90** 176101

[81] Stroscio J A and Celotta R J 2004 Controlling the dynamics of a single atom in lateral atom manipulation *Science* **306** 242

[82] Stroscio J A, Tavazza F, Crain J N, Celotta R J and Chaka A M 2006 Electronically induced atom motion in engineered $CoCu_n$ nanostructures *Science* **313** 984

[83] Kogan A, Amasha S, Goldhaber-Gordon D, Granger G, Kastner M A and Shtrikman H 2004 Measurements of Kondo and spin splitting in single-electron transistors *Phys. Rev. Lett.* **93** 166602

[84] Hirjibehedin C F, Lin C-Y, Otte A F, Ternes M, Lutz C P, Jones B A and Heinrich A J 2007 Large magnetic anisotropy of a single atomic spin embedded in a surface molecular network *Science* **317** 1199

[85] Lorente N, Persson M, Lauhon L J and Ho W 2001 Symmetry selection rules for vibrationally inelastic tunneling *Phys. Rev. Lett.* **86** 2593

[86] Hofer W A, Teobaldi G and Lorente N 2008 Creating pseudo-Kondo resonances by field-induced diffusion of atomic hydrogen *Nanotechnology* **19** 305701

[87] Lipus K, Bachem E and Urban W 1991 Vibration-rotation spectroscopy of the CrH radical in its X 6 $\sigma+$ ground state by CO-Faraday laser magnetic resonance *Mol. Phys.* **73** 1041

[88] Ram R S and Bernath P F 1996 Fourier transform emission spectroscopy of new infrared systems of LaH and LaD *J. Chem. Phys.* **104** 6444

[89] Liu K and Gao S 2006 Adsorbate vibration and resonance lifetime broadening of a cobalt adatom on a Cu(111) surface *Phys. Rev.* B **74** 195433

[90] Witte G 2002 Low frequency vibrational modes of adsorbates *Surf. Sci.* **502** 405

[91] Hofer W A, Palotás K, Rusponi S, Cren T and Brune H 2008 Role of hydrogen in giant spin polarization observed on magnetic nanostructures *Phys. Rev. Lett.* **100** 026806

[92] Temirov R, Soubatch S, Neucheva O, Lassise A C and Tautz F S 2008 A novel method achieving ultra-high geometrical resolution in scanning tunnelling microscopy *New J. Phys.* **10** 053012

[93] Abrikosov A A and Gor'kov L P 1962 *Sov. Phys.—JETP* **15** 1088

[94] Yazdani A, Jones B A, Lutz C P, Crommie M F and Eigler D M 1997 Probing the local effects of magnetic impurities on superconductivity *Science* **275** 1767

[95] Bürgi L 1999 Scanning tunneling microscopy as local probe of electron density, dynamics, and transport at metall surface *PhD Thesis* École Polytechnique Fédérale de Lausanne http://library.epfl.ch/theses/?nr=2033

[96] Bardeen J, Cooper L N and Schrieffer J R 1957 Theory of superconductivity *Phys. Rev.* **108** 1175

[97] Pan S H, Hudson E W and Davis J C 1998 Vacuum tunneling of superconducting quasiparticles from atomically sharp scanning tunneling microscope tips *Appl. Phys. Lett.* **73** 2992

[98] Dynes R C, Narayanamurti N and Garno J P 1978 Direct measurement of quasiparticle-lifetime broadening in a strong-coupled superconductor *Phys. Rev. Lett.* **41** 1509

[99] Tersoff J and Hamann D R 1983 Theory and application for the scanning tunneling microscope *Phys. Rev. Lett.* **50** 1998

[100] Tersoff J and Hamann D R 1985 Theory of the scanning tunneling microscope *Phys. Rev.* B **31** 805

[101] Pan S H, Hudson E W, Lang K M, Eisaki H, Uchida S and Davis J C 2000 Imaging the effects of individual zinc impurity atoms on superconductivity in $Bi_2Sr_2CaCu_2O_{8+\delta}$ *Nature* **403** 746

[102] Ji S H, Zhang T, Fu Y-S, Chen X, Ma X-C, Li J, Duan W-H, Jia J-F and Xue Q-K 2008 High-resolution scanning tunneling spectroscopy of magnetic impurity induced bound states in the superconducting gap of pb thin films *Phys. Rev. Lett.* **100** 226801

[103] Ternes M, Schneider W-D, Cuevas J C, Lutz C P, Hirjibehedin C F and Heinrich A J 2006 Subgap structure in asymmetric superconducting tunnel junctions *Phys. Rev.* B **74** 132501

[104] Salkola M I, Balatsky A V and Schrieffer J R 1997 Spectral properties of quasiparticle excitations induced by magnetic moments in superconductors *Phys. Rev.* B **55** 12648

[105] Šmakov J, Martin I and Balatsky A V 2002 Theory of scanning tunneling microscopy measurement of single spin decoherence in a superconductor *Phys. Rev. Lett.* **88** 037003

[106] Anderson P W 1959 Theory of dirty superconductors *J. Phys. Chem. Solids* **11** 26

[107] Shiba H 1968 Classical spins in superconductors *Prog. Theor. Phys.* **40** 435

[108] Flatté M E and Byers J M 1997 Local electronic structure of a single magnetic impurity in a superconductor *Phys. Rev. Lett.* **78** 3761

[109] Andersson M, Cuevas J C and Fogelström M 2002 Transport through superconductor/magnetic dot/superconductor structures *Physica* C **367** 117

[110] Odom T W, Huang J-L, Cheung C L and Lieber C M 2000 Magnetic clusters on single-walled carbon nanotubes: the Kondo effect in a one-dimensional host *Science* **290** 1549

[111] Qiu X H, Nazin G V and Ho W 2003 Vibrationally resolved fluorescence excited with submolecular precision *Science* **299** 542

[112] Ćavar E, Blüm M-C, Pivetta M, Patthey F, Chergui M and Schneider W-D 2005 Fluorescence and phosphorescence from individual C_{60} molecules excited by local electron tunneling *Phys. Rev. Lett.* **95** 196102
[113] Hirjibehedin C F, Lutz C P and Heinrich A J 2006 Spin coupling in engineered atomic structures *Science* **312** 1021
[114] Leibsle F M, Dhesi S S, Barrett S D and Robinson A W 1994 STM observations of Cu(100)c(2 × 2)N surfaces: evidence for attractive interactions and an incommensurate c(2 × 2) structure *Surf. Sci.* **317** 309
[115] Park J *et al* 2002 Coulomb blockade and the Kondo effect in single-atom transistors *Nature* **417** 722
[116] Liang W, Shores M P, Bockrath M, Long J R and Park H 2002 Kondo resonance in a single-molecule transistor *Nature* **417** 725
[117] Shen L Y L and Rowell J M 1968 Zero-bias tunneling anomalies-temperature, voltage, and magnetic field dependence *Phys. Rev.* **165** 566
[118] Wegewijs M R, Romeike C, Schoeller H and Hofstetter W 2007 Magneto-transport through single-molecule magnets: Kondo-peaks, zero-bias dips, molecular symmetry and Berry's phase *New J. Phys.* **9** 344
[119] Žitko R, Peters R and Pruschke Th 2008 Properties of anisotropic magnetic impurities on surfaces *Phys. Rev.* B submitted (arXiv:0809.0759)
[120] Ruderman M A and Kittel C 1954 Indirect exchange coupling of nuclear magnetic moments by conduction electrons *Phys. Rev.* **96** 99
[121] Kasuya T 1956 A theory of metallic ferro-and antiferromagnetism on Zener's model *Prog. Theor. Phys.* **16** 45
[122] Yosida K 1957 Magnetic properties of Cu–Mn alloys *Phys. Rev.* **106** 893
[123] Van Vleck J H 1962 Note on the interactions between the spins of magnetic ions or nuclei in metals *Rev. Mod. Phys.* **34** 681
[124] Stepanyuk V S, Niebergall L, Longo R C, Hergert W and Bruno P 2004 Magnetic nanostructures stabilized by surface-state electrons *Phys. Rev.* B **70** 075414
[125] Chen W, Jamneala T, Madhavan V and Crommie M F 1999 Disappearance of the Kondo resonance for atomically fabricated cobalt dimers *Phys. Rev.* B **60** R8529
[126] Jamneala T, Madhavan V and Crommie M F 2001 Kondo response of a single antiferromagnetic chromium trimer *Phys. Rev. Lett.* **87** 256804
[127] Wahl P, Simon P, Diekhöner L, Stepanyuk V S, Bruno P, Schneider M A and Kern K 2007 Exchange interaction between single magnetic adatoms *Phys. Rev. Lett.* **98** 056601
[128] Brovko O O, Ignatiev P A, Stepanyuk V S and Bruno P 2008 Tailoring exchange interactions in engineered nanostructures: an *ab initio* study *Phys. Rev. Lett.* **101** 036809
[129] Yayon Y, Brar V W, Senapati L, Erwin S C and Crommie M F 2007 Observing spin polarization of individual magnetic adatom *Phys. Rev. Lett.* **99** 067202
[130] Meier F, Zhou L, Wiebe J and Wiesendanger R 2008 Revealing magnetic interactions from single-atom magnetization curves *Science* **320** 82
[131] Jeong H, Chang A M and Melloch M R 2001 The Kondo effect in an artificial quantum dot molecule *Science* **293** 2221
[132] Heersche H B, de Groot Z, Folk J A, Kouwenhoven L P and van der Zant H S J 2006 Kondo effect in the presence of magnetic impurities *Phys. Rev. Lett.* **96** 017205
[133] Otte A F 2008 Magnetism of a Single Atom *PhD Thesis* Universiteit Leiden https://openaccess.leidenuniv.nl/handle/1887/12660